Chem

Article

Analysis of kinetic asymmetry in a multi-cycle reaction network establishes the principles for autonomous compartmentalized molecular ratchets

Graphical abstract

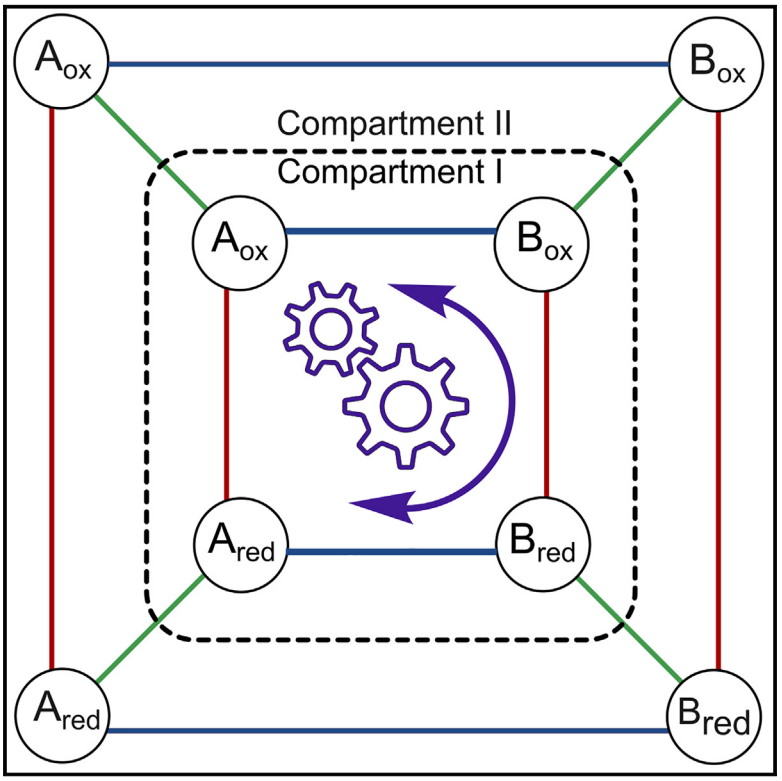

Highlights

- We describe how to calculate kinetic asymmetry in multi-cycle networks
- Compartmentalization enables energy ratchet effects as only light was believed to do
- Herein, thermodynamics alone can control directionality in autonomous molecular ratchets
- Differences in diffusion properties result in information ratchet effects

Authors

Emanuele Penocchio, Ahmad Bachir, Alberto Credi, Raymond Dean Astumian, Giulio Ragazzon

Correspondence

emanuele.penocchio@northwestern.edu (E.P.),
astumian@maine.edu (R.D.A.),
ragazzon@unistra.fr (G.R.)

In brief

The single most important parameter describing a chemical non-equilibrium system is, arguably, kinetic asymmetry. This work generalizes its expression to multi-cycle networks. Building on this advancement, we investigate the role of compartmentalization in driving systems away from equilibrium, revealing that compartmentalization enables features so far associated only with light-driven systems. In particular, under the conditions considered, thermodynamics alone dictates the directionality of a chemical reaction network under non-equilibrium conditions.

Penocchio et al., 2024, Chem *10*, 3644–3655
December 12, 2024
https://doi.org/10.1016/j.chempr.2024.07.038

CellPress

CellPress
OPEN ACCESS

Chem

Article

Analysis of kinetic asymmetry in a multi-cycle reaction network establishes the principles for autonomous compartmentalized molecular ratchets

Emanuele Penocchio,[1,6,*] Ahmad Bachir,[2,6] Alberto Credi,[3,4] Raymond Dean Astumian,[2,5,*] and Giulio Ragazzon[2,7,*]
[1]Department of Chemistry, Northwestern University, Evanston, IL 60208, USA
[2]Institut de Science et d'Ingénierie Supramoléculaires (ISIS), University of Strasbourg, CNRS, 8 allée Gaspard Monge, 67000 Strasbourg, France
[3]CLAN-Center for Light Activated Nanostructures, Istituto per la Sintesi Organica e la Fotoreattività, Consiglio Nazionale delle Ricerche, Via Gobetti 101, 40129 Bologna, Italy
[4]Dipartimento di Chimica Industriale "Toso Montanari", Università di Bologna, Viale del Risorgimento 4, 40136 Bologna, Italy
[5]Department of Physics and Astronomy, University of Maine, Orono, ME 04469, USA
[6]These authors contributed equally
[7]Lead contact
*Correspondence: emanuele.penocchio@northwestern.edu (E.P.), astumian@maine.edu (R.D.A.), ragazzon@unistra.fr (G.R.)
https://doi.org/10.1016/j.chempr.2024.07.038

THE BIGGER PICTURE Life is a complex, non-equilibrium chemical phenomenon, and kinetic asymmetry is arguably the most significant parameter to describe non-equilibrium chemical reaction networks, helping to unravel and engineer such systems. However, its description is currently limited to very simple networks. In this work, we generalize the calculation of kinetic asymmetry virtually to any network. We use this generalization to formalize the theory of non-equilibrium operation enabled by spatial separation, using a recently reported redox-driven multi-cycle system as a concrete example. Thus, we offer a new perspective on the central role of compartmentalization in biology and its importance in sustaining living organisms away from equilibrium.

SUMMARY

Kinetic asymmetry is a key parameter describing non-equilibrium systems: it indicates the directionality of a reaction network under steady-state conditions. So far, kinetic asymmetry has been evaluated only in networks featuring a single cycle. Here, we have investigated kinetic asymmetry in a multi-cycle system using a combined theoretical and numerical approach. First, we report the general expression of kinetic asymmetry for multi-cycle networks. Then, we specify it for a recently reported electrochemically controlled network comprising diffusion steps, which we used as a model system to reveal how key parameters influence directionality. In contrast with the current understanding, we establish that spatial separation—including compartmentalization—can enable autonomous energy ratchet mechanisms, with directionality dictated by thermodynamic features. Kinetic simulations confirm analytical findings and illustrate the interplay between diffusion, chemical, and electrochemical processes. The treatment is general, as it can be applied to other multi-cycle networks, facilitating the realization of endergonic processes across domains.

INTRODUCTION

Operating away from equilibrium is a key feature of life and holds great promise for developing chemical systems with advanced functionalities.[1–4] Ultimately, a non-equilibrium chemical system can be described as a chemical reaction network exchanging energy with its surroundings.[5–8] When the reactions of the network can occur continuously under constant environmental conditions in the presence of a steady energy supply, the system is said to be autonomous.[9,10] A key property to describe the dynamics of a such a network is kinetic asymmetry,[11,12] which is quantified by the ratcheting constant K_r and reports on the directionality of the chemical reaction network at the steady state. The concept of kinetic asymmetry has been used to rationalize the operation of chemically driven autonomous molecular motors,[12–19] non-equilibrium self-assembly,[20–23] chemotaxis,[24,25] and non-reciprocal interactions,[26] as well as several other processes requiring an energy input to occur, i.e., that are endergonic.[27,28]

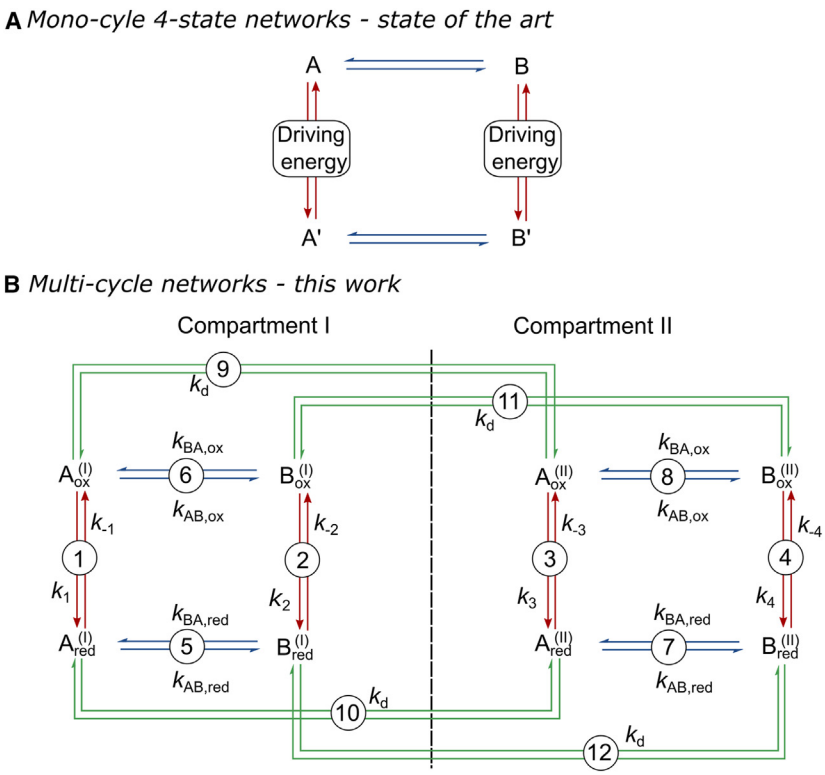

Figure 1. Chemical reactions networks

(A) A 4-species mono-cycle chemical reaction network.

(B) The 8-species multi-cycle chemical reaction network[35] discussed in this work, obtained upon forming two compartments divided by an ideal permeable membrane (dashed). Without loss of generality, we identify reactions as proceeding in the positive direction when going from ox to red in the case of redox reactions, from (B) to (A) in the case of chemical reactions, and from compartment I to compartment II within the model in the case of diffusion processes.

(C) Illustration of an experimental example that can be rationalized using the present approach, comprising a redox-active host-guest system; self-assembly and redox reactions would form a square reaction network in the vicinity of each electrode; the shaded states and reactions are less relevant than others experimentally. In all panels, reactions are color-coded, with red steps exchanging energy with the source, blue steps indicating chemical reactions, and green steps representing diffusion across the permeable barrier. Back and forth harpoons are used to denote equilibrium transitions.[36]

So far, the description of kinetic asymmetry in chemical reaction networks has focused on cyclic networks having a single cycle, i.e., networks where the relevant cyclic sequence of reactions involves all intermediates present in the system.[12,20,29–33] In these networks, kinetic asymmetry can be expressed as the product of the reactions' rates along the cycle in one direction over the product of the rates in the opposite direction.[27] Crucially, up to now it has always been considered that when single-cycle networks operate under time-independent environmental conditions, kinetic asymmetry can only emerge from differences in transition-state energies within an information ratchet mechanism.[27] The intrinsic thermodynamic stability of intermediates is relevant only when light is used as an energy source, thus making photochemical systems the sole framework in which one can implement an autonomous energy ratchet effect, i.e., a mechanism where directionality is dictated solely by the thermodynamic stability of intermediates.[34] However, this simple description breaks down when only some of the species participate in the relevant reaction cycle, which is the subject of this work (Figure 1). In this situation, multiple cycles can contribute to kinetic asymmetry.

Multi-cycle chemical reaction networks are extremely common—especially in systems chemistry. Yet, very little work has been focused on their kinetic asymmetry, and, in general, the directionality has been assigned based on experimental observations complemented by system-specific analyses. Multi-cycle systems are fairly easy to realize experimentally: a simple strategy is to consider a system having two switchable properties (e.g., redox state and conformation), resulting in a square reaction network such as the one shown in Figure 1A. Including the possibility of diffusing between two spatially distinguished locations affords the network shown in Figure 1B. We decided to investigate this network—as a specific case of how multi-cycle networks might arise—because it represents the logical extension of widely explored square schemes and offers insights on the underlying principles of spatially distinguished systems, i.e., systems that are not uniform in space.

The same type of network can also describe a recent experimental example, where a redox process and a self-assembly reaction were combined with diffusion to obtain an autonomous system powered by electrical energy.[37] As sketched in Figure 1C,

the authors operated the redox-switchable host-guest system between the electrodes of a scanning electrochemical microscope, which allowed the simultaneous promotion of oxidation and reduction at two independently controlled electrodes. This condition is gaining attention and has already demonstrated its potential in surface and material science,[38,39] offering an alternative to alternating redox potentials or scanning tunneling microscopy experiments.[40–43] In the work focused on autonomous operation, the authors used experimental data and kinetic simulations to support the idea that the system's operation was predominantly controlled by an autonomous energy ratchet mechanism.[37] Such an autonomous operation mechanism was previously described in detail exclusively in relation to light-driven systems,[44–46] and, as a result, the theoretical basis for such a mechanism remains unexplored in relation to ground-state reactivity.[47]

Here, we present the treatment of kinetic asymmetry in a representative case of a multi-cycle network. In particular, we focused on a redox-powered network, closely mapping the one underlying the recently reported autonomous electrically driven system, to investigate the origin of its somewhat unconventional ratchet mechanism. We identify a regime where directionality is solely controlled by thermodynamic features of the system, while the kinetics of diffusion processes should be intermediate between other processes. This solves a significant controversy in the chemical literature: can the direction of cycling through a sequence of reactions be controlled by an equilibrium constant—i.e., by the relative free energies of some of the states—or is it under purely kinetic control? Previous analyses on cyclic processes without mass transport (diffusion or flow between several spatially distinct locations) have suggested that directionality is always under kinetic control. Here, we could demonstrate the possibility of controlling directionality via equilibrium constants by generalizing the analytical calculation of kinetic asymmetry to multi-cycle systems. Furthermore, we describe how the non-equilibrium pumping equality—a key result of trajectory thermodynamics for kinetically asymmetric systems—manifests itself in multi-cycle networks with mass transport.

Our work establishes the principles for spatially distinguished autonomous molecular ratchets, which emerge as the sole alternative to light-driven systems to dictate directionality using thermodynamic properties. Analytical results are validated by numerical simulations, which we also use to show that diffusion rates can be tuned to implement an information ratchet mechanism within the same system. Although we focus on a specific case study, our approach is general and can be used to analyze kinetic asymmetry in virtually any multi-cycle chemical reaction network. Finally, we stress that we kept mathematical treatments to a minimum in the main text. Interested readers can refer to the supplemental information for the full step-by-step analysis.

RESULTS AND DISCUSSION

Model system

To describe spatial separation, one can either treat space continuously or introduce compartments, with diffusion processes modeled as a set of additional reactions modeling how species move from one compartment to the other.[27] Here, we chose to introduce compartments to remain in the realm of chemical reaction networks and link spatially distinguished systems with compartmentalized systems—where a physical barrier separates the compartments—that constitute a sub-set of spatially distinguished systems. The system depicted in Figure 1B is controlled by two electrodes, and the two compartments model the proximity to them. Adding a third middle compartment would help to distinguish the bulk solution separating the electrodes, mapping the experimental setup even closer, but we use just two compartments as they suffice to illustrate the general principles investigated. In compartment I, species are closer to electrode I, which is kept at potential E_I. In compartment II, species are closer to electrode II. Within each compartment, the concentrations are considered uniform. Species can diffuse between the two compartments according to first-order processes controlled by diffusion constants k_d (reactions 9, 10, 11, and 12 in Figure 1B).

In each of the two compartments, the same 4-species square reaction network is present, resulting from orthogonal redox and chemical processes. Species A and B can interconvert thermally via reactions 5, 6, 7, and 8 in Figure 1B. The oxidized species $\mathbf{A}_\mathrm{ox}$ and $\mathbf{B}_\mathrm{ox}$ are converted to their reduced counterparts $\mathbf{A}_\mathrm{red}$ and $\mathbf{B}_\mathrm{red}$ via electrochemical reactions 1, 2, 3, and 4 occurring at the two electrodes (Figure 1B). The thermodynamic properties of the reactions forming a square cycle are related by the microscopic reversibility constraint:

$$K_\mathrm{ox}K_\mathrm{red}^{-1} = \frac{k_\mathrm{BA,ox}}{k_\mathrm{AB,ox}}\frac{k_\mathrm{AB,red}}{k_\mathrm{BA,red}} = e^{(F/RT)\left(E_\mathrm{B}^0 - E_\mathrm{A}^0\right)} = e^{(F/RT)\Delta E^0} \quad \text{(Equation 1)}$$

where K_ox and K_red are the equilibrium constants of the chemical reactions, each defined as $K = k_\mathrm{BA}/k_\mathrm{AB}$; F and R the Faraday and the gas constants, respectively; T the temperature; and E^0s the standard redox potentials of species A and B.

The rate of redox processes is described by Butler-Volmer kinetics, the standard approach for describing heterogeneous electron transfer.[48] In essence, the equilibrium populations of $\mathbf{A}_\mathrm{ox}$ and $\mathbf{A}_\mathrm{red}$ (and, analogously, $\mathbf{B}_\mathrm{ox}$, $\mathbf{B}_\mathrm{red}$) in each compartment depend on the standard redox potential of this redox couple ($E_\mathrm{A}{}^0$) and the potential applied to the electrode, which therefore can be used to control their relative thermodynamic stability within a compartment. When the potentials of the two electrodes differ, an electrochemical potential gradient $\Delta E = E_\mathrm{II} - E_\mathrm{I}$ is established between the two compartments and energy is available to drive the system away from equilibrium.

We note that the investigated model consists of only unimolecular chemical reactions, but because kinetic asymmetry is a steady-state property, our findings also extend to systems that feature bimolecular self-assembly reactions. Indeed, concentrations are constant at the steady-state, which allows describing bimolecular self-assembly reactions as pseudo-first-order processes. This consideration is relevant also to the experimental system that inspired this work, which comprises self-assembly steps.[37] The parallel of our model with the experimental setup is further reinforced by the absence of convection and migration

phenomena, which are routinely excluded under the relevant experimental conditions.

General analytical treatment

From a chemical perspective, it is interesting to understand when the transport of electrons can influence other reactions that are, in principle, unrelated to the redox process. In the present case, it is a matter of understanding whether the chemical reactions 5, 6, 7, and 8 interconverting A and B can use some of the energy provided by the electric current via redox reactions 1, 2, 3, and 4 to depart from equilibrium and generate a directed net flux across the chemical reaction network. This type of energy transduction can take place once there is a sequence of steps that makes two different processes happen simultaneously (not in sequence). For example, here the sequence of reactions $1 \rightarrow -5 \rightarrow 12 \rightarrow -4 \rightarrow -11$ (see the caption of Figure 1B for the notation and sign convention) transfers one electron from electrode I to electrode II and simultaneously converts $\mathbf{A}_{ox}$ in $\mathbf{B}_{ox}$. In line with literature on molecular machines,[10,27,28,49] we refer to this condition as the *coupling* of the redox reactions to the chemical steps, while being aware that the same term is used also with less technically stringent meaning in the broader chemical literature. Promoting coupled chemical reactions is the outcome of an operating ratchet mechanism.[27,28] In practice, an operative ratchet mechanism would imply that the conversion of **A** into **B** happens preferentially in one redox state, say, in the reduced state (i.e., a net flux $\mathbf{A}_{red} \rightarrow \mathbf{B}_{red}$, independently of the compartment), and that the conversion of **B** into **A** occurs in the other redox state, say, in the oxidized state. If this were the case, then cycling through the network according to the sequence of reactions S: $\mathbf{A}_{ox} \rightarrow \mathbf{A}_{red} \rightarrow \mathbf{B}_{red} \rightarrow \mathbf{B}_{ox} \rightarrow \mathbf{A}_{ox}$ would have a different probability than the reversed sequence: S^{-1}: $\mathbf{A}_{ox} \leftarrow \mathbf{A}_{red} \leftarrow \mathbf{B}_{red} \leftarrow \mathbf{B}_{ox} \leftarrow \mathbf{A}_{ox}$. Therefore, sequence S describes the coupling of the redox reactions to the chemical steps. In this particular network, sequence S is the only coupling that can arise; more than one coupled sequence may be present in more complex systems.

At the steady state, the overall directional bias for the sequence S, namely the kinetic asymmetry of the chemical reaction network, can be quantified as the ratio between the (average) frequencies at which sequences S and S^{-1} are traveled. Such a ratio is typically called "ratcheting constant," K_r, or "directionality," r_0, and quantifies kinetic asymmetry. K_r is a non-equilibrium constant quantifying the kinetic preference for traveling the sequence S with respect to S^{-1}. In particular, $K_r > 1$ denotes a preference for sequence S, $K_r < 1$ denotes a preference for sequence S^{-1}, and $K_r = 1$ denotes the absence of a kinetic bias in the system, a condition often referred to as "kinetic symmetry," corresponding, in this case, to the chemical reactions not being coupled to the inter-electrode current. Mathematically, K_r can be computed by dividing the sum of the frequencies (j) of all the cycles realizing the sequence S by the sum of the frequencies of all the cycles realizing S^{-1}. Therefore, to quantify kinetic asymmetry, we need to identify all the cycles that contribute to S and S^{-1}, which can be of three types, differing in how they are coupled to the energy source.

Slip cycles,[29] R_i (a letter chosen to avoid confusion with the sequence S), realize sequence S without moving any net number of electrons between the electrodes. An example is the counterclockwise cycle $1 \rightarrow -5 \rightarrow -2 \rightarrow 6$, where the counterclockwise direction refers to the representation in Figure 1B. These cycles are not associated with a net exchange of energy, therefore their microscopic reverse cycles (such as clockwise $-6 \rightarrow 2 \rightarrow 5 \rightarrow -1$) are equally likely and thus slip cycles do not give a net contribution to directionality.

The forward cycles, F_i, are those cycles realizing the sequence S and concomitantly moving one electron from electrode I to electrode II. For example, the counterclockwise cycle $1 \rightarrow -5 \rightarrow 12 \rightarrow -4 \rightarrow 8 \rightarrow -9$ is a forward cycle. The frequency with which this cycle is traveled with respect to its microscopic reverse (clockwise $9 \rightarrow -8 \rightarrow 4 \rightarrow -12 \rightarrow 5 \rightarrow -1$) is controlled by the electrochemical potential gradient. In particular, forward cycles are $e^{(F/RT)\Delta E}$ times faster than the corresponding microscopic reverses. This relation implies that, in the absence of a gradient ($\Delta E = 0$), no energy is exchanged across the cycle and no preferred directionality emerges, while forward cycles directly contribute to directionality in the presence of a gradient.

The backward cycles, B_i, realize the sequence S^{-1} and concomitantly move one electron from electrode I to electrode II. For example, the cycle $-8 \rightarrow -11 \rightarrow 2 \rightarrow 5 \rightarrow 10 \rightarrow -3$ is a backward cycle. As in the case of forward cycles, a net electron current is associated with the cycle, and a contribution to directionality can arise in the presence of a gradient.

After some algebraic passages (see supplemental information section 2.1), K_r can be expressed as:

$$K_r = \frac{q + e^{-(F/RT)\Delta E} + \Gamma}{q e^{-(F/RT)\Delta E} + 1 + \Gamma} \qquad \text{(Equation 2)}$$

with

$$q = \frac{\sum_i j_{F_i}}{\sum_i j_{B_i}} \qquad \text{(Equation 3)}$$

$$\Gamma = \frac{\sum_i j_{R_i}}{\sum_i j_{B_i}} \qquad \text{(Equation 4)}$$

where J_{X_i} denotes the frequency of cycle X_i and summations are intended to run over all the forward, backward, and slip cycles.

This expression of K_r—derived in the context of electrochemical systems—takes the exact same form[29,47,50] that characterizes catalysis-driven systems, where the chemical potential gradient of the catalyzed reaction plays the role of ΔE, thus offering a unified treatment of ratchet mechanisms in the ground state. Equation 2 contains only three system-specific parameters: ΔE, q, and Γ, which are solely responsible for directionality. Their meaning is intuitive: ΔE reflects the energy available to drive the non-equilibrium process; q compares the forward and backward cycles (promoting S or S^{-1}, respectively), thus reporting on the overall kinetic bias; and Γ reports on the relative weight of slip cycles, which do not contribute directly to directionality. We can use this reasoning to interpret a few mathematical relations derived from Equation 2 (see the supplemental information section 2.1 for proof). When $\Delta E = 0$, the numerator and denominator become equal, and $K_r = 1$;

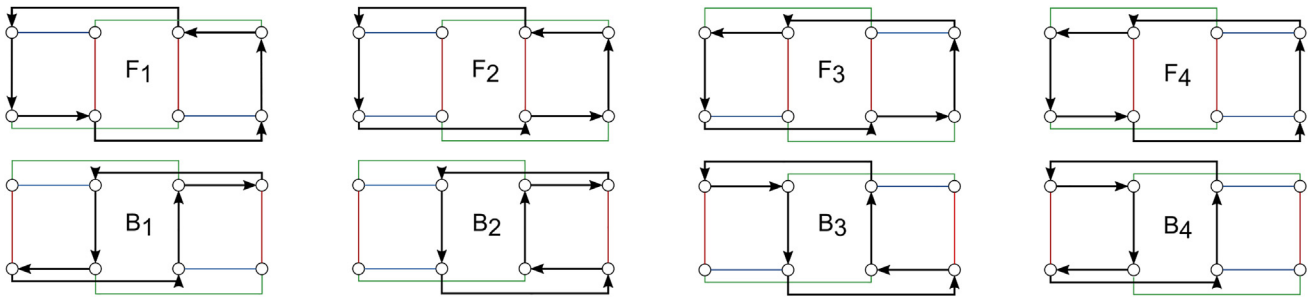

Figure 2. Representation of forward and backward cycles

Cycles indicated by black arrows move one electron from compartment I (left) to compartment II (right), while realizing the sequence S (forward cycles, F_i) or the sequence S^{-1} (backward cycles, B_i). The network species, reactions, and color-coding coincide with those reported in Figure 1B; e.g., the top-left species is $\mathbf{A}_{ox}^{(I)}$ and the leftmost vertical connection corresponds to reaction 1 in Figure 1B.

therefore, no directionality can emerge, reiterating the necessity of an energy source. Directionality is also suppressed when Γ—appearing both in the numerator and denominator—is large. The larger Γ, the closer to 1 K_r will be, meaning that the slip cycles dominate and the inter-electrode current is only weakly coupled to the chemical reactions. In the limit of $\Gamma \to 0$, known as the complete coupling regime,[47] the effectiveness of the ratchet mechanism is maximized as chemical reactions will almost always happen concurrently to electron transport. Focusing on the effect of q, when $\Delta E > 0$, K_r will be greater (smaller) than 1 if $q >$ (<)1. On the contrary, when $\Delta E < 0$, K_r will be greater (smaller) than 1 if $q <$ (>)1. In the context of catalysis-driven systems, the overall kinetic bias q is related to the difference in the transitions states' free energy between the forward and backward cycles and is sometimes called the "Curtin-Hammett asymmetry factor" (denoted $F_{C\text{-}H}$) in light of its connections with kinetic resolution.[50] As a recent experimental investigation showed,[51] having $q \neq 1$ does not necessarily imply an experimentally observable kinetic asymmetry (K_r) because the latter can be overwhelmed by the occurrence of slip cycles. Here, the kinetic bias is intrinsically related to the thermodynamic bias via the Butler-Volmer equation and its interplay with spatial differentiation. In redox reactions, the interplay between kinetics and thermodynamics may also be non-linear, as occurring, for example, in the reactions described by Marcus theory of electron transfer; we note that implementing such reaction kinetics would afford non-equilibrium systems characterized by a negative differential response.[52]

Diagram method for cycles' frequencies

The analysis presented so far is valid for any chemical reaction network controlled by electrochemical reactions occurring at two electrodes. In fact, an identical approach can be used to describe any multi-cycle network, even besides electrochemically driven and spatially distinguished systems. Now, we detail how the general treatment applies to the specific network of Figure 1B.

To compute q, we need to identify all cycles of type F_i and B_i and compute the corresponding frequencies. The present network has four F_i and four B_i cycles, illustrated in Figure 2. The procedure used to calculate cycles' frequencies is based on a diagram method derived from graph theory.[53–55] In particular, we adopted the notation illustrated in Hill.[56] We anticipate that the frequency j associated to a given cycle X_i—as well as any other cycle considered here—can be expressed in the following form:

$$j_{X_i} = \frac{\Pi_{X_i} \Sigma_{X_i}}{N} \qquad \text{(Equation 5)}$$

N is a normalizing constant common to all the cycles; it simplifies out when computing q, and its explicit computation is therefore not necessary here. The term Π_{X_i} is the product of all the rate constants involved in the cycle. Heuristically, it can be thought of as a measure of how fast the cycle X_i is traveled on average; the same terms also appear in the computation of kinetic asymmetry in mono-cycle networks.

The Σ_{X_i} term only appears in multi-cycle networks and can be thought of as a factor expressing the probability of entering cycle X_i. Mathematically, Σ_{X_i} is the sum of the contributions from all the so-called "rooted spanning trees"[55] of cycle X_i. A rooted spanning tree is a sequence of reactions entering the cycle starting from all the species not included in the cycle (without forming new cycles).

Cycle F_1 corresponds to the most important cycle in the reference experimental case (compare Figures 1C and 2). Therefore, we take it as an example and depict all its rooted spanning trees in Figure 3. The contribution to Σ_{F_1} of each spanning tree is the product of the rate constants involved, as shown in Figure 3, Σ_{F_1} being the sum of the contributions from all the spanning trees. The detailed mathematical expression of terms Π_{X_i} and Σ_{X_i} for all the relevant cycles are reported in the supplemental information.

Autonomous energy ratchet operation

From now on, with the intent of seeking purely energy ratchet effects, we purposely exclude kinetic biases by considering all species as having the same diffusion constant k_d and charge-transfer coefficient, a realistic regime for the experimental systems that inspired this work (see supplemental information section 1).[37]

Computing all Π_{X_i} terms reveals that all Π_{F_i} and Π_{B_i} terms are equal. This finding can be used (see supplemental information section 2.2) to simplify the general expression of q into the following system-specific form:

$$q = \frac{\Sigma_{F_1} + \Sigma_{F_2} + \Sigma_{F_3} + \Sigma_{F_4}}{\Sigma_{B_1} + \Sigma_{B_2} + \Sigma_{B_3} + \Sigma_{B_4}} \quad \text{(Equation 6)}$$

This expression contains only spanning tree terms—peculiar to multi-cycle systems—which are evidently essential in controlling directionality. In particular, the sums at the numerator and denominator take the following expressions:

$$\Sigma_{F_1} + \Sigma_{F_2} + \Sigma_{F_3} + \Sigma_{F_4} = \left(e^{(F/2RT)\Delta E} e^{(F/2RT)\Delta E^0} + 1\right) \times C_1 + \left(e^{(F/RT)\Delta E} e^{(F/RT)\Delta E^0} + 1\right) \times C_2 + C_3 \quad \text{(Equation 7)}$$

$$\Sigma_{B_1} + \Sigma_{B_2} + \Sigma_{B_3} + \Sigma_{B_4} = \left(e^{(F/2RT)\Delta E} + e^{(F/2RT)\Delta E^0}\right) \times C_1 + \left(e^{(F/RT)\Delta E} + e^{(F/RT)\Delta E^0}\right) \times C_2 + C_3 \quad \text{(Equation 8)}$$

where parameters C_{1-3} are functions of the rate constants and electrochemical potentials characterizing the network, for example:

$$C_3 = (k_{BA,ox} + k_{AB,ox} + 2k_d) \times (k_{BA,red} + k_{AB,red} + 2k_d) \quad \text{(Equation 9)}$$

where $k_{AB,ox(red)}$ is the rate constant for the formation of **B** in the oxidized (reduced state) and $k_{BA,ox(red)}$ is its microscopic reverse (see Figure 1B). The expressions of parameter C_1 and C_2 are reported in the supplemental information.

Given the final form of Equations 7 and 8, it can be demonstrated (see supplemental information section 2.2 for the proof) that ratio q in Equation 6 will be larger or smaller than 1, depending on the sign of $\Delta E \times \Delta E^0$, thus the electrochemical potential gradient ΔE and the difference in standard redox potentials ΔE^0 control q. Specifically, q is > 1 if $\Delta E \times \Delta E^0 > 0$, and q is < 1 if $\Delta E \times \Delta E^0 < 0$. Because ΔE and ΔE^0 control q, it may seem that they both control directionality, K_r, expressed by Equation 2. However, because Equation 2 contains q and ΔE both at the numerator and the denominator, the sign of ΔE does not influence directionality. As a result, ΔE^0 is the sole quantity responsible for directionality in the investigated network: if $K_{ox} > K_{red}$ ($\Delta E^0 > 0$), then any applied voltage, regardless of its sign, favors cycling in the order S, and if $K_{ox} < K_{red}$ ($\Delta E^0 < 0$), then any applied voltage favors cycling in the order S^{-1}. ΔE^0 is intrinsic to the system at study, and inherently related to the equilibrium constant of the chemical reactions by the microscopic reversibility constraint reported in Equation 1. At any given potential difference other than zero between the electrodes, directionality is dictated by thermodynamic features, a hallmark of energy ratchet mechanisms. Yet, ΔE can be controlled externally simply by changing electrode potentials. As a result, both the driving force and magnitude of directionality can be modulated at will, which is considerably harder—and sometimes even practically impossible—to achieve in systems powered by chemical energy or light.

Additional insights are offered by the expression of parameter C_3 (Equation 9), which is the only term contributing to q that is independent from ΔE and ΔE^0. If diffusion is much faster than chemical reactions, C_3 dominates the ratio in Equation 6, and directionality vanishes. Therefore, chemical reactions should be faster than diffusion for an optimal q value. However, when diffusion is too slow, slip cycles become dominant (e.g., the sequence $1 \rightarrow -5 \rightarrow -2 \rightarrow 6$, entirely occurring in the cathodic compartment, *vide supra*). Mathematically, this is reflected in larger values of Γ, which suppress directionality according to Equation 2.

Non-equilibrium species concentration

The occurrence of a non-equilibrium steady-state—featuring directional reaction fluxes—implies a concentration imbalance with respect to equilibrium. Comparing concentrations in the presence and the absence of energy inputs is often a viable experimental measure to probe the coupling's effectiveness. In this particular case, it is insightful to compare the total amounts of species A and B in the oxidized and reduced state. If the chemical reactions were at equilibrium, those ratios would equal K_{ox} and K_{red}, respectively. Therefore, values different from the corresponding equilibrium constant are signatures of the coupling. We can express those ratios using the same analytical treatment we used to express K_r (see Figure S1 and related discussion). After some algebraic passages (see supplemental information section 2.3), we find:

$$\frac{\left[A_{red}^{(I)}\right] + \left[A_{red}^{(II)}\right]}{\left[B_{red}^{(I)}\right] + \left[B_{red}^{(II)}\right]} = K_{red} \times \left\{\frac{q + e^{-(F/RT)\Delta E} + \psi_{red}}{q e^{-(F/RT)\Delta E} + 1 + \psi_{red}}\right\} \quad \text{(Equation 10)}$$

$$\frac{\left[A_{ox}^{(I)}\right] + \left[A_{ox}^{(II)}\right]}{\left[B_{ox}^{(I)}\right] + \left[B_{ox}^{(II)}\right]} = K_{ox} \times \left\{\frac{q e^{-(F/RT)\Delta E} + 1 + \psi_{ox}}{q + e^{-(F/RT)\Delta E} + \psi_{ox}}\right\} \quad \text{(Equation 11)}$$

The above equations show that the same parameters controlling directionality also control concentration ratios. In fact, the terms in brackets are closely related to K_r in Equation 2. When $K_r = 1$, equivalent to $\Delta E = 0$ and/or $\Delta E^\circ = 0$ (leading to $q = 1$, see discussion in the previous section), the terms in brackets are also unitary, leading to no concentration imbalance with respect to equilibrium. When $K_r > 1$, equivalent to $\Delta E \neq 0$ and $\Delta E^\circ > 0$ (leading to $q > 1$), chemical reactions depart from equilibrium, favoring $\mathbf{A}_{red}$ and $\mathbf{B}_{ox}$ species over $\mathbf{B}_{red}$ and $\mathbf{A}_{ox}$, respectively. When $K_r < 1$, equivalent to $\Delta E \neq 0$ and $\Delta E^\circ < 0$ (leading to $q < 1$), non-equilibrium conditions favor $\mathbf{B}_{red}$ and $\mathbf{A}_{ox}$ species over $\mathbf{A}_{red}$ and $\mathbf{B}_{ox}$, respectively. In other words, as with cycling direction, species' relative abundances can be electrochemically driven toward non-equilibrium values, and the sign of the effect can be engineered only based on the relative magnitude of the equilibrium constants K_{ox} and K_{red} (controlling ΔE^0). The two new parameters appearing in Equations 10 and 11, ψ_{ox}

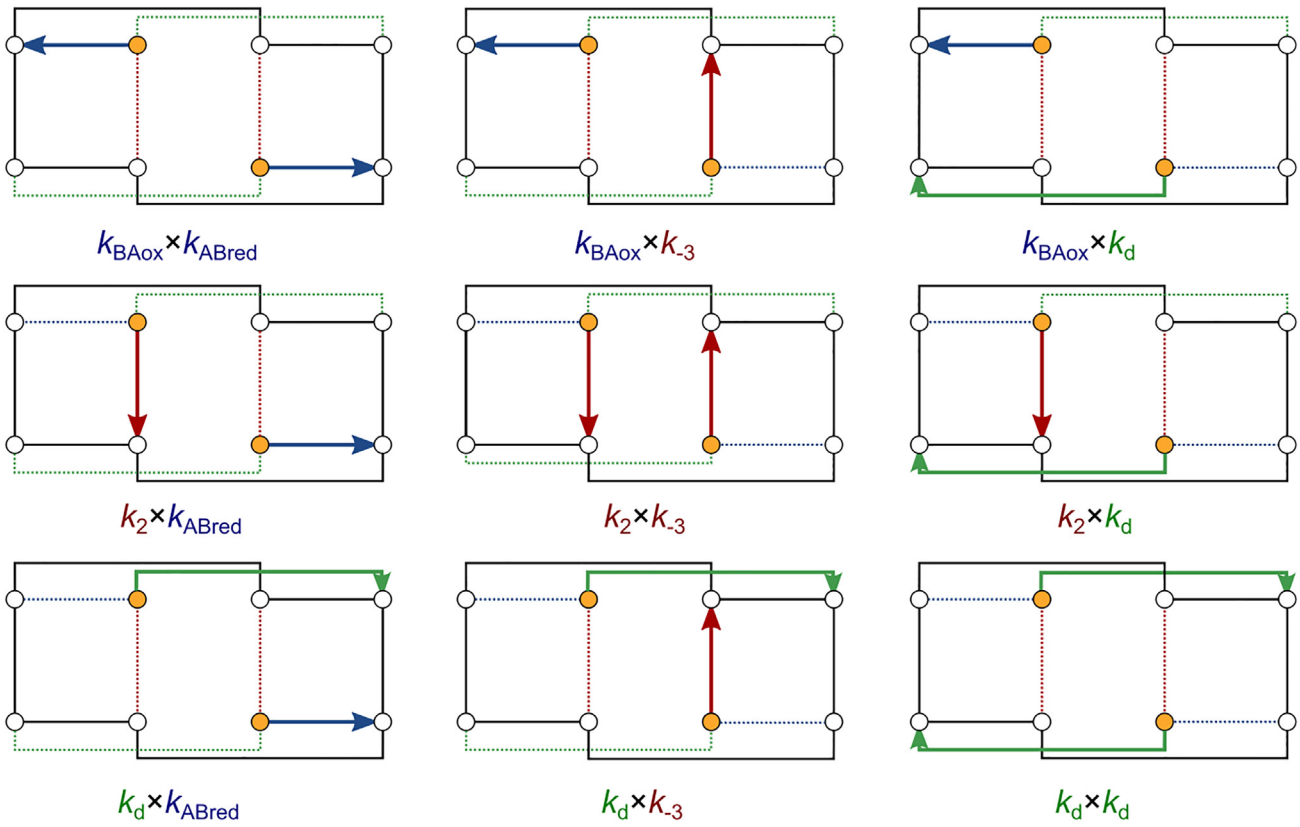

Figure 3. Rooted spanning trees for cycle F_1

The corresponding contributions to Σ_{F_1} are indicated below their graphical representation. Cycle F_1 is reported in black, the species not included in the cycle are indicated in orange. The network species, reactions, and color-coding coincide with those reported in Figures 1B and 2.

and ψ_{red}, are analogous to Γ in Equation 2 in that they report on the effectiveness of the ratchet mechanism (see supplemental information section 2.3 for their analytical expressions). Namely, for large ψs, non-equilibrium ratios will remain close to the corresponding equilibrium ratios, making the coupling poor.

Equations 10 and 11 are instances of the non-equilibrium pumping equality:[57,58]

$$\frac{[j]}{[i]} = K_{ij}\langle e^{\mathcal{W}_{s_{ij}}/RT}\rangle \qquad \text{(Equation 12)}$$

a general result from trajectory thermodynamics that relates the steady-state concentration ratio between two species, i and j, to the exponential of the path-dependent energy exchanged with the environment, $\mathcal{W}_{s_{ij}}$, in each specific trajectory, s_{ij}, kinetically weighted and averaged over all trajectories between those two species. The factor $\langle e^{\mathcal{W}_{s_{ij}}/RT}\rangle$ is not straightforward to compute explicitly in complicated networks. Here, we could provide an analytical expression by leveraging graph-theoretical techniques, as detailed in the supplemental information. The ratcheting constant K_r and the non-equilibrium pumping equality epitomize the fundamental role of kinetic asymmetry, here reflected in the parameter q, for harnessing energy and realizing functions out of equilibrium.

Numerical investigation

To investigate the impact of our findings on a plausible system, we assigned reasonable values to the parameters characterizing the investigated network and performed numerical simulations to investigate the effect of network parameters and confirm the analytical predictions. Chemical reactions were imposed having a rate in the order of 1–100 s^{-1}, which is somewhat slower than typical NMR timescales. A reduction potential of −0.2 V was selected for species **A**, which is close to the reduction potential of the viologen species involved in the experimental study that inspired this work.[37] Because all reactions involved follow a first-order kinetic, the model system is insensitive to the total species concentration. Significantly, the diffusion constants k_d differ from typical diffusion values because here they report on the propensity of species to change compartment and not their actual propensity to move in space. In most cases, under the simulation conditions, electrode I serves as a cathode, promoting species reduction, while electrode II serves as an anode, promoting oxidation.

The results obtained from exploring the dependence of chemical reactions' fluxes (net conversion from **B** to **A**) on electrode potentials, equilibrium constants, and diffusion constants are reported in Figures 4A–4D and S2–S5.

When both electrodes have the same potential (−0.2 V), there are no reaction fluxes (i.e., the system reaches equilibrium). On

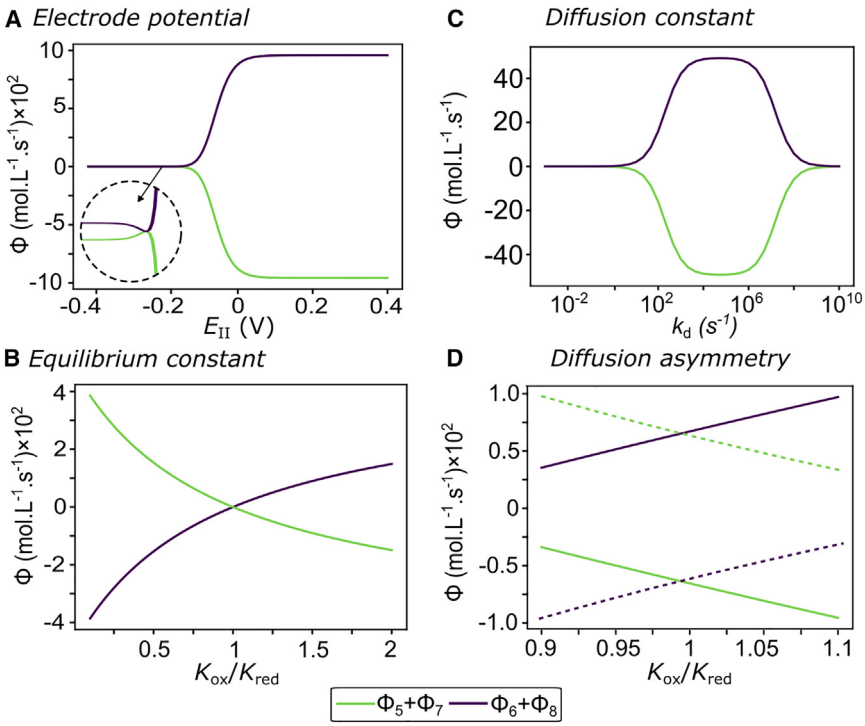

Figure 4. Dependence of reaction fluxes on model parameters

(A) Electrode potential. The inset magnifies the system behavior around $\Delta E = 0$, showing that the cycling direction is unaffected by the sign of ΔE and is only dictated by thermodynamic features, as predicted by our theoretical analysis.

(B) Equilibrium constants of chemical reactions.

(C) Diffusion coefficient.

(D) Diffusion asymmetry, obtained slowing down by 1,000 times species (B) (full lines) or species (A) (dashed lines), and observed in proximity to $K_{ox}/K_{red} = 1$, where fluxes are zero in the absence of diffusion asymmetry. According to the above equations, a positive flux indicates that the conversion from (B) to (A) is dominant over the opposite process. Details of numerical simulation are given in the text and supplemental information section 3 (see Tables S1–S3 for simulation parameters).

In all panels, the fluxes 5, 6, 7, and 8 are simulated using these expressions: ($\Phi_5 = k_{BA,red}\,[B_{red}^{(I)}] - k_{AB,red}\,[A_{red}^{(I)}]$; $\Phi_6 = k_{BA,ox}\,[B_{ox}^{(I)}] - k_{AB,ox}\,[A_{ox}^{(I)}]$; $\Phi_7 = k_{BA,red}\,[B_{red}^{(II)}] - k_{AB,red}\,[A_{red}^{(II)}]$; $\Phi_8 = k_{BA,ox}\,[B_{ox}^{(II)}] - k_{AB,ox}\,[A_{ox}^{(II)}]$).

the contrary, when E_{II} becomes more positive, directional reaction fluxes emerge that reach a plateau slightly above the E_B^0. If the E_{II} becomes more negative than E_I, lower than the cathode, the fluxes maintain their sign (Figure 4A), in line with the general analytical treatment presented above identifying ΔE^0 as the sole determinator of directionality. Yet, the magnitude of fluxes is significantly different, with an approximate 10^6-times difference between the two plateaus observed. Modulation of the equilibrium constants affords results in line with the analytical findings, reporting a current inversion around equilibrium constant equality (Figure 4B). In this case, the fluxes' magnitude is symmetrical with respect to the energetic imbalance imposed (see Figure S2C for the logarithmic plot). The observed behavior is reminiscent of Tafel plots, which relate current and overpotential: this observation is less surprising when realizing that changing the equilibrium constant also changes the redox potential—to respect the detailed balance constraint in Equation 1—and thus the overpotential. Because fluxes and concentration imbalances are directly related, the same numerical results also corroborate the analytical findings discussing non-equilibrium concentrations. (see Figure S5 for the explicit numerical verification of Equations 10 and 11).

Changing the diffusion coefficient over twelve orders of magnitude revealed the bell-shaped curve predicted by the network-specific analytical treatment (Figure 4C). The onset of fluxes occurs close to $k_d = 1$, with fluxes reaching a plateau above $k_d = 10^2$. These values coincide with the rate constants associated with chemical reactions, the slowest processes in the network. Instead, the fluxes vanish around $k_d = 10^6$, which is comparable with rates of redox processes, the fastest reactions in the network. Therefore, chemical and electrochemical parameters control the shape of the bell curve. This interpretation was corroborated by simulations in which the shape of the bell was selectively modulated by changing chemical and electrochemical parameters. For example, slowing all the chemical reactions by one order of magnitude shifts only the low-diffusion flux onset, while speeding up all the redox processes analogously shifted only the high-diffusion flux onset (see Figure S3). A similar reasoning might apply to the bell-shaped profile predicted for the turnover frequency associated with heterogeneous catalysis occurring under alternating conditions.[59,60] However, we remain careful in drawing a strict parallel between spatial and temporal differentiation as a means to alternate different conditions because here the variation is stochastic and not collective. In this regard, the parallel is much closer between spatially separated systems and light-driven systems operated under continuous irradiation, for which the analogy works well. We also note that, in the present case, the region characterized by high diffusion constants and low fluxes seems, however, hard to investigate experimentally, as it falls close to the nanosecond timescale. Interestingly, simulations performed that kept both electrodes at negative potentials (Figures S4A–S4C) illustrated that fluxes are also observed when both electrodes are kept at potentials lower than the redox potential of both species involved. Because the occurrence of a directional flux implies the absorption of energy from a source, this phenomenon might be used to harvest energy from any potential difference, acquiring a broader significance.

Finally, we took advantage of numerical simulation to investigate the effect of diffusion asymmetry.[25] To this aim, we imposed a different diffusion constant for species **A** with respect to species B. In this case, even in the absence of a thermodynamic

bias, a directional current was observed, which was reversed when the diffusion asymmetry was reversed (Figure 4D). On the contrary, differentiating the rates of chemical reactions did not produce analogous effects (Figures S4D and S4E). These simulations indicate that diffusion asymmetry can give rise to a pure information ratchet effect and imply that, in spatially distinguished systems, energy and information ratchet effects can coexist.[27,61] Indeed, diffusion asymmetry was present in the experimental example discussed above[37]; however, the difference in diffusion coefficients was modest (1.5 times) and directionality remained dictated by thermodynamic stabilities. In line with experimental evidence and simulations, systems involving supramolecular polymers[23] or metabolons[62] would more easily present properties stemming from diffusion asymmetry compared with small-molecule systems. Overall, the numerical simulations corroborated analytical results and allowed us to gain additional insights, specifically on the factors controlling the bell-shaped profile of fluxes vs. diffusion constant and the additional opportunities opened by diffusion asymmetry, whose detailed investigation goes beyond the scope of the present article.

Conclusions

This work unlocks the description of kinetic asymmetry in multi-cycle networks. The analytical treatment leading to Equation 2 and the diagrammatic method to find cycles' frequencies are general and can be applied[63] to any multi-cycle chemical reaction network, even besides electrochemically driven and spatially distinguished systems. Here, we focused on a spatially distinguished system powered by redox reactions and leveraged it to establish the theoretical basis for autonomous energy ratchet mechanisms enabled by spatial separation, including compartmentalization. The characteristic features of this broadly applicable ratchet mechanism are the following: (1) when $\Delta E = 0$ (no driving) or when $\Delta E^0 = 0$ (i.e., $K_{ox} = K_{red}$), no energy ratchet mechanism is active and chemical steps are predicted to be at equilibrium (no net current); (2) having $\Delta E \neq 0$ is not sufficient to impart directionality in the network, as an overall kinetic bias ($q \neq 1$) is also necessary, and the sequence S is traveled preferentially in the forward (backward) direction if $\Delta E^0 > (<)0$, namely the sign of the effect can be engineered based on $K_{ox}/K_{red} > (<)1$, a thermodynamic parameter; and (3) fast diffusion is predicted to hamper directionality and reduce the current across the chemical reactions, with slow diffusion predicted to maintain directionality but also reduce currents by slowing down cycles' fluxes. On top of anticipating reaction fluxes, the same treatment has been used to predict non-equilibrium concentrations, an often experimentally accessible quantity. This prediction was obtained by retrieving the non-equilibrium pumping equality by leveraging graph-theoretical techniques. The analytical findings have been corroborated by numerical simulations, which also revealed the processes controlling the bell-shaped profile features. Although the mathematical treatment focused entirely on an energy ratchet mechanism, simulations allow introducing diffusion asymmetry, which installs an information ratchet effect, showing that energy and information ratchet effects can coexist in spatially distinguished autonomous systems. This feature is also found in light-driven systems, where continuous irradiation converts molecules stochastically between different states, regardless of the thermodynamic stability of each intermediate. Our findings have implications for the development of endergonic processes across domains of chemistry, from metabolism[51] and redox-active systems[64–67] to molecular machines,[40,68] chemotaxis, and compartmentalization,[69–71] also in a prebiotic environment,[72–74] as well as the development of soft materials,[75,76] thermo-electrochemical cells,[77,78] sensing,[79] and surface pattering under non-equilibrium conditions.[80]

EXPERIMENTAL PROCEDURES

Resource availability

Lead contact

Further information and requests for resources should be directed to and will be fulfilled by the lead contact, Giulio Ragazzon (ragazzon@unistra.fr).

Materials availability

This study did not generate new materials.

Data and code availability

The code used to generate numerical simulations is available upon request.

ACKNOWLEDGMENTS

This work was supported by the Interdisciplinary Thematic Institute (ITI-CSC) via the IdEx Unistra (ANR-10-IDEX-0002) within the program Investissement d'avenir and the European Research Council (ERC-2021-StG 101041933 – KI-NET to G.R.). A.B. thanks the CSC Graduate School funded by the French National Research Agency (CSC-IGS ANR-17-EURE-0016) and the Region Grand Est (ACTION 15 SESRI – Volet 2, 22-DOC-065) for a PhD fellowship. The authors would like to thank Benjamin M.W. Roberts, Massimo Bilancioni, and Joaquin B. Buye for their insightful comments.

AUTHOR CONTRIBUTIONS

E.P. and A.B. contributed equally. Conceptualization, E.P., R.D.A., A.C., and G.R.; formal analysis, E.P. and A.B.; validation, E.P., R.D.A., and G.R.; writing, E.P., A.B., and G.R., with input from R.D.A. and A.C.; funding, G.R.

DECLARATION OF INTERESTS

The authors declare no competing interests.

SUPPLEMENTAL INFORMATION

Supplemental information can be found online at https://doi.org/10.1016/j.chempr.2024.07.038.

Received: April 21, 2024
Revised: June 28, 2024
Accepted: July 30, 2024
Published: September 13, 2024

REFERENCES

1. Mattia, E., and Otto, S. (2015). Supramolecular systems chemistry. Nat. Nanotechnol. *10*, 111–119. https://doi.org/10.1038/nnano.2014.337.
2. Grzybowski, B.A., and Huck, W.T.S. (2016). The nanotechnology of life-inspired systems. Nat. Nanotechnol. *11*, 585–592. https://doi.org/10.1038/nnano.2016.116.
3. Walther, A. (2019). Viewpoint: From Responsive to Adaptive and Interactive Materials and Materials Systems: A Roadmap. Adv. Mater. *32*, e1905111. https://doi.org/10.1002/adma.201905111.

4. Kaspar, C., Ravoo, B.J., van der Wiel, W.G., Wegner, S.V., and Pernice, W.H.P. (2021). The rise of intelligent matter. Nature *594*, 345–355. https://doi.org/10.1038/s41586-021-03453-y.

5. Qian, H., and Beard, D.A. (2005). Thermodynamics of stoichiometric biochemical networks in living systems far from equilibrium. Biophys. Chem. *114*, 213–220. https://doi.org/10.1016/j.bpc.2004.12.001.

6. Le Saux, T.T., Plasson, R.R., and Jullien, L.L. (2014). Energy propagation throughout chemical networks. Chem. Commun. *50*, 6189–6195. https://doi.org/10.1039/c4cc00392f.

7. Rao, R., and Esposito, M. (2016). Nonequilibrium thermodynamics of chemical reaction networks: Wisdom from stochastic thermodynamics. Phys. Rev. X *6*, 1–23. https://doi.org/10.1103/PhysRevX.6.041064.

8. Brown, A.I., and Sivak, D.A. (2020). Theory of Nonequilibrium Free Energy Transduction by Molecular Machines. Chem. Rev. *120*, 434–459. https://doi.org/10.1021/acs.chemrev.9b00254.

9. Kay, E.R., and Leigh, D.A. (2015). Rise of the Molecular Machines. Angew. Chem. Int. Ed. *54*, 10080–10088. https://doi.org/10.1002/anie.201503375.

10. Baroncini, M., Silvi, S., and Credi, A. (2020). Photo- And Redox-Driven Artificial Molecular Motors. Chem. Rev. *120*, 200–268. https://doi.org/10.1021/acs.chemrev.9b00291.

11. Astumian, R.D., Chock, P.B., Tsong, T.Y., and Westerhoff, H.V. (1989). Effects of oscillations and energy-driven fluctuations on the dynamics of enzyme catalysis and free-energy transduction. Phys. Rev. A *39*, 6416–6435. https://doi.org/10.1103/physreva.39.6416.

12. Astumian, R.D. (2019). Kinetic asymmetry allows macromolecular catalysts to drive an information ratchet. Nat. Commun. *10*, 3837. https://doi.org/10.1038/s41467-019-11402-7.

13. Kay, E.R., Leigh, D.A., and Zerbetto, F. (2007). Synthetic molecular motors and mechanical machines. Angew. Chem. Int. Ed. *46*, 72–191. https://doi.org/10.1002/anie.200504313.

14. Wilson, M.R., Solà, J., Carlone, A., Goldup, S.M., Lebrasseur, N., and Leigh, D.A. (2016). An autonomous chemically fuelled small-molecule motor. Nature *534*, 235–240. https://doi.org/10.1038/nature18013.

15. Pezzato, C., Cheng, C., Stoddart, J.F., and Astumian, R.D. (2017). Mastering the non-equilibrium assembly and operation of molecular machines. Chem. Soc. Rev. *46*, 5491–5507. https://doi.org/10.1039/c7cs00068e.

16. Kassem, S., Van Leeuwen, T., Lubbe, A.S., Wilson, M.R., Feringa, B.L., and Leigh, D.A. (2017). Artificial molecular motors. Chem. Soc. Rev. *46*, 2592–2621. https://doi.org/10.1039/c7cs00245a.

17. Amano, S., Fielden, S.D.P., and Leigh, D.A. (2021). A catalysis-driven artificial molecular pump. Nature *594*, 529–534. https://doi.org/10.1038/s41586-021-03575-3.

18. Borsley, S., Kreidt, E., Leigh, D.A., and Roberts, B.M.W. (2022). Autonomous fuelled directional rotation about a covalent single bond. Nature *604*, 80–85. https://doi.org/10.1038/s41586-022-04450-5.

19. Borsley, S., Leigh, D.A., and Roberts, B.M.W. (2024). Molecular Ratchets and Kinetic Asymmetry: Giving Chemistry Direction. Angew. Chem. Int. Ed. *63*, e202400495. https://doi.org/10.1002/anie.202400495.

20. Ragazzon, G., and Prins, L.J. (2018). Energy consumption in chemical fuel-driven self-assembly. Nat. Nanotechnol. *13*, 882–889. https://doi.org/10.1038/s41565-018-0250-8.

21. Penocchio, E., Rao, R., and Esposito, M. (2019). Thermodynamic efficiency in dissipative chemistry. Nat. Commun. *10*, 3865. https://doi.org/10.1038/s41467-019-11676-x.

22. Das, K., Gabrielli, L., and Prins, L.J. (2021). Chemically Fueled Self-Assembly in Biology and Chemistry. Angew. Chem. Int. Ed. *60*, 20120–20143. https://doi.org/10.1002/anie.202100274.

23. Sharko, A., Livitz, D., De Piccoli, S., Bishop, K.J.M., and Hermans, T.M. (2022). Insights into Chemically Fueled Supramolecular Polymers. Chem. Rev. *122*, 11759–11777. https://doi.org/10.1021/acs.chemrev.1c00958.

24. Feng, M., and Gilson, M.K. (2020). Enhanced Diffusion and Chemotaxis of Enzymes. Annu. Rev. Biophys. *49*, 87–105. https://doi.org/10.1146/annurev-biophys-121219-081535.

25. Mandal, N.S., Sen, A., and Astumian, R.D. (2023). Kinetic Asymmetry versus Dissipation in the Evolution of Chemical Systems as Exemplified by Single Enzyme Chemotaxis. J. Am. Chem. Soc. *145*, 5730–5738. https://doi.org/10.1021/jacs.2c11945.

26. Mandal, N.S., Sen, A., and Astumian, R.D. (2024). A molecular origin of non-reciprocal interactions between interacting active catalysts. Chem *10*, 1147–1159. https://doi.org/10.1016/j.chempr.2023.11.017.

27. Sangchai, T., Al Shehimy, S., Penocchio, E., and Ragazzon, G. (2023). Artificial Molecular Ratchets: Tools Enabling Endergonic Processes. Angew. Chem. Int. Ed. *62*, e202309501. https://doi.org/10.1002/anie.202309501.

28. Borsley, S., Gallagher, J.M., Leigh, D.A., and Roberts, B.M.W. (2024). Ratcheting synthesis. Nat. Rev. Chem. *8*, 8–29. https://doi.org/10.1038/s41570-023-00558-y.

29. Astumian, R.D. (2015). Irrelevance of the power stroke for the directionality, stopping force, and optimal efficiency of chemically driven molecular machines. Biophys. J. *108*, 291–303. https://doi.org/10.1016/j.bpj.2014.11.3459.

30. Amano, S., Esposito, M., Kreidt, E., Leigh, D.A., Penocchio, E., and Roberts, B.M.W.W. (2022). Insights from an information thermodynamics analysis of a synthetic molecular motor. Nat. Chem. *14*, 530–537. https://doi.org/10.1038/s41557-022-00899-z.

31. Penocchio, E., and Ragazzon, G. (2023). Kinetic Barrier Diagrams to Visualize and Engineer Molecular Nonequilibrium Systems. Small *19*, e2206188. https://doi.org/10.1002/smll.202206188.

32. Corra, S., Bakić, M.T., Groppi, J., Baroncini, M., Silvi, S., Penocchio, E., Esposito, M., and Credi, A. (2022). Kinetic and energetic insights into the dissipative non-equilibrium operation of an autonomous light-powered supramolecular pump. Nat. Nanotechnol. *17*, 746–751. https://doi.org/10.1038/s41565-022-01151-y.

33. Binks, L., Borsley, S., Gingrich, T.R., Leigh, D.A., Penocchio, E., and Roberts, B.M.W. (2023). The role of kinetic asymmetry and power strokes in an information ratchet. Chem *9*, 2902–2917. https://doi.org/10.1016/j.chempr.2023.05.035.

34. Astumian, R.D., and Derényi, I. (1998). Fluctuation driven transport and models of molecular motors and pumps. Eur. Biophys. J. *27*, 474–489. https://doi.org/10.1007/s002490050158.

35. Astumian, R.D., Chock, P.B., Tsong, T.Y., Chen, Y.D., and Westerhoff, H.V. (1987). Can free energy be transduced from electric noise? Proc. Natl. Acad. Sci. USA *84*, 434–438. https://doi.org/10.1073/pnas.84.2.434.

36. Aprahamian, I., and Goldup, S.M. (2023). Non-equilibrium Steady States in Catalysis, Molecular Motors, and Supramolecular Materials: Why Networks and Language Matter. J. Am. Chem. Soc. *145*, 14169–14183. https://doi.org/10.1021/jacs.2c12665.

37. Ragazzon, G., Malferrari, M., Arduini, A., Secchi, A., Rapino, S., Silvi, S., and Credi, A. (2023). Autonomous Non-Equilibrium Self-Assembly and Molecular Movements Powered by Electrical Energy. Angew. Chem. Int. Ed. *62*, e202214265. https://doi.org/10.1002/anie.202214265.

38. Krabbenborg, S.O.O., Veerbeek, J., and Huskens, J. (2015). Spatially Controlled Out-of-Equilibrium Host-Guest System under Electrochemical Control. Chem. Eur. J. *21*, 9638–9644. https://doi.org/10.1002/chem.201501544.

39. Barpuzary, D., Hurst, P.J., Patterson, J.P., and Guan, Z. (2023). Waste-Free Fully Electrically Fueled Dissipative Self-Assembly System. J. Am. Chem. Soc. *145*, 3727–3735. https://doi.org/10.1021/jacs.2c13140.

40. Pezzato, C., Nguyen, M.T., Kim, D.J., Anamimoghadam, O., Mosca, L., and Stoddart, J.F. (2018). Controlling Dual Molecular Pumps Electrochemically. Angew. Chem. Int. Ed. *57*, 9325–9329. https://doi.org/10.1002/anie.201803848.

41. Tierney, H.L., Murphy, C.J., Jewell, A.D., Baber, A.E., Iski, E.V., Khodaverdian, H.Y., McGuire, A.F., Klebanov, N., and Sykes, E.C.H. (2011).

Experimental demonstration of a single-molecule electric motor. Nat. Nanotechnol. *6*, 625–629. https://doi.org/10.1038/nnano.2011.142.

42. Perera, U.G.E., Ample, F., Kersell, H., Zhang, Y., Vives, G., Echeverria, J., Grisolia, M., Rapenne, G., Joachim, C., and Hla, S.W. (2013). Controlled clockwise and anticlockwise rotational switching of a molecular motor. Nat. Nanotechnol. *8*, 46–51. https://doi.org/10.1038/nnano.2012.218.
43. Pumm, A.K., Engelen, W., Kopperger, E., Isensee, J., Vogt, M., Kozina, V., Kube, M., Honemann, M.N., Bertosin, E., Langecker, M., et al. (2022). A DNA origami rotary ratchet motor. Nature *607*, 492–498. https://doi.org/10.1038/s41586-022-04910-y.
44. Koumura, N., Zijlstra, R.W.J., van Delden, R.A., Harada, N., and Feringa, B.L. (1999). Light-driven monodirectional molecular rotor. Nature *401*, 152–155. https://doi.org/10.1038/43646.
45. Serreli, V., Lee, C.-F., Kay, E.R., and Leigh, D.A. (2007). A molecular information ratchet. Nature *445*, 523–527. https://doi.org/10.1038/nature05452.
46. Ragazzon, G., Baroncini, M., Silvi, S., Venturi, M., and Credi, A. (2015). Light-powered autonomous and directional molecular motion of a dissipative self-assembling system. Nat. Nanotechnol. *10*, 70–75. https://doi.org/10.1038/nnano.2014.260.
47. Astumian, R.D. (2024). Kinetic Asymmetry and Directionality of Nonequilibrium Molecular Systems. Angew. Chem. Int. Ed. *63*, e202306569. https://doi.org/10.1002/anie.202306569.
48. Bard, A.J., and Faulkner, L.R. (2001). Electrochemical Methods, 2nd Edition (John Wiley & Sons).
49. Erbas-Cakmak, S., Leigh, D.A., McTernan, C.T., and Nussbaumer, A.L. (2015). Artificial Molecular Machines. Chem. Rev. *115*, 10081–10206. https://doi.org/10.1021/acs.chemrev.5b00146.
50. Amano, S., Esposito, M., Kreidt, E., Leigh, D.A., Penocchio, E., and Roberts, B.M.W. (2022). Using Catalysis to Drive Chemistry Away from Equilibrium: Relating Kinetic Asymmetry, Power Strokes, and the Curtin-Hammett Principle in Brownian Ratchets. J. Am. Chem. Soc. *144*, 20153–20164. https://doi.org/10.1021/jacs.2c08723.
51. Marchetti, T., Roberts, B.M.W.W., Frezzato, D., and Prins, L.J. (2024). A Minimalistic Covalent Bond-Forming Chemical Reaction Cycle that Consumes Adenosine Diphosphate. Angew. Chem. Int. Ed. *63*, e202402965. https://doi.org/10.1002/anie.202402965.
52. Falasco, G., Cossetto, T., Penocchio, E., and Esposito, M. (2019). Negative differential response in chemical reactions. New J. Phys. *21*, 73005. https://doi.org/10.1088/1367-2630/ab28be.
53. King, E.L., and Altman, C. (1956). A schematic method of deriving the rate laws for enzyme-catalyzed reactions. J. Phys. Chem. *60*, 1375–1378. https://doi.org/10.1021/j150544a010.
54. Hill, T.L. (1966). Studies in irreversible thermodynamics. IV. diagrammatic representation of steady state fluxes for unimolecular systems. J. Theor. Biol. *10*, 442–459. https://doi.org/10.1016/0022-5193(66)90137-8.
55. Nam, K.M., Martinez-Corral, R., and Gunawardena, J. (2022). The linear framework: Using graph theory to reveal the algebra and thermodynamics of biomolecular systems. Interface Focus *12*, 20220013. https://doi.org/10.1098/rsfs.2022.0013.
56. Hill, T.L. (1989). Free Energy Transduction and Biochemical Cycle Kinetics (Springer-Verlag). https://doi.org/10.1007/978-1-4612-3558-3.
57. Astumian, R.D., and Robertson, B. (1993). Imposed oscillations of kinetic barriers can cause an enzyme to drive a chemical reaction away from equilibrium. J. Am. Chem. Soc. *115*, 11063–11068. https://doi.org/10.1021/ja00077a001.
58. Astumian, R.D. (2018). Trajectory and Cycle-Based Thermodynamics and Kinetics of Molecular Machines: The Importance of Microscopic Reversibility. Acc. Chem. Res. *51*, 2653–2661. https://doi.org/10.1021/acs.accounts.8b00253.
59. Shetty, M., Walton, A., Gathmann, S.R., Ardagh, M.A., Gopeesingh, J., Resasco, J., Birol, T., Zhang, Q., Tsapatsis, M., Vlachos, D.G., et al. (2020). The Catalytic Mechanics of Dynamic Surfaces: Stimulating Methods for Promoting Catalytic Resonance. ACS Catal. *10*, 12666–12695. https://doi.org/10.1021/acscatal.0c03336.
60. Foley, B.L., and Razdan, N.K. (2024). Clarifying mechanisms and kinetics of programmable catalysis. iScience *27*, 109543. https://doi.org/10.1016/j.isci.2024.109543.
61. Sabatino, A., Penocchio, E., Ragazzon, G., Credi, A., and Frezzato, D. (2019). Individual-Molecule Perspective Analysis of Chemical Reaction Networks: The Case of a Light-Driven Supramolecular Pump. Angew. Chem. Int. Ed. *58*, 14341–14348. https://doi.org/10.1002/anie.201908026.
62. Zhao, X., Palacci, H., Yadav, V., Spiering, M.M., Gilson, M.K., Butler, P.J., Hess, H., Benkovic, S.J., and Sen, A. (2018). Substrate-driven chemotactic assembly in an enzyme cascade. Nat. Chem. *10*, 311–317. https://doi.org/10.1038/nchem.2905.
63. Yang, Z., Wang, X., Penocchio, E., Ragazzon, G., Chen, X., Lu, S., Zhou, Y., Fu, K., Liu, Z., Cai, Y., et al. (2024). Beyond Single-Cycle Autonomous Molecular Machines: Light-Powered Shuttling in a Multi-Cycle Reaction Network. Angew. Chem. Int. Ed. *2024*, e202414072. https://doi.org/10.1002/anie.202414072.
64. Leira-Iglesias, J., Tassoni, A., Adachi, T., Stich, M., and Hermans, T.M. (2018). Oscillations, travelling fronts and patterns in a supramolecular system. Nat. Nanotechnol. *13*, 1021–1027. https://doi.org/10.1038/s41565-018-0270-4.
65. Del Grosso, E., Ponzo, I., Ragazzon, G., Prins, L.J., and Ricci, F. (2020). Disulfide-Linked Allosteric Modulators for Multi-cycle Kinetic Control of DNA-Based Nanodevices. Angew. Chem. Int. Ed. *59*, 21058–21063. https://doi.org/10.1002/anie.202008007.
66. Howlett, M.G., Engwerda, A.H.J.J., Scanes, R.J.H.H., and Fletcher, S.P. (2022). An autonomously oscillating supramolecular self-replicator. Nat. Chem. *14*, 805–810. https://doi.org/10.1038/s41557-022-00949-6.
67. Gentile, S., Del Grosso, E., Prins, L.J., and Ricci, F. (2023). Autonomous and Programmable Reorganization of DNA-Based Polymers Using Redox Chemistry. Chem. Eur. J. *29*, e202300394. https://doi.org/10.1002/chem.202300394.
68. Zhang, L., Qiu, Y., Liu, W.G., Chen, H., Shen, D., Song, B., Cai, K., Wu, H., Jiao, Y., Feng, Y., et al. (2023). An electric molecular motor. Nature *613*, 280–286. https://doi.org/10.1038/s41586-022-05421-6.
69. Borsley, S., Haugland, M.M., Oldknow, S., Cooper, J.A., Burke, M.J., Scott, A., Grantham, W., Vallejo, J., Brechin, E.K., Lusby, P.J., and Cockroft, S.L. (2019). Electrostatic Forces in Field-Perturbed Equilibria: Nanopore Analysis of Cage Complexes. Chem *5*, 1275–1292. https://doi.org/10.1016/j.chempr.2019.03.004.
70. Zhang, Y., and Hess, H. (2021). Chemically-powered swimming and diffusion in the microscopic world. Nat. Rev. Chem. *5*, 500–510. https://doi.org/10.1038/s41570-021-00281-6.
71. Borsley, S. (2024). Membrane Transport, Molecular Machines, and Maxwell's Demon. ChemSystemsChem *6*, e202400004. https://doi.org/10.1002/syst.202400004.
72. Branscomb, E., Biancalani, T., Goldenfeld, N., and Russell, M. (2017). Escapement mechanisms and the conversion of disequilibria; the engines of creation. Phys. Rep. *677*, 1–60. https://doi.org/10.1016/j.physrep.2017.02.001.
73. Ianeselli, A., Salditt, A., Mast, C., Ercolano, B., Kufner, C.L., Scheu, B., and Braun, D. (2023). Physical non-equilibria for prebiotic nucleic acid chemistry. Nat. Rev. Phys. *5*, 185–195. https://doi.org/10.1038/s42254-022-00550-3.
74. Muchowska, K.B., Varma, S.J., and Moran, J. (2020). Nonenzymatic Metabolic Reactions and Life's Origins. Chem. Rev. *120*, 7708–7744. https://doi.org/10.1021/acs.chemrev.0c00191.
75. Moulin, E., Faour, L., Carmona-Vargas, C.C., and Giuseppone, N. (2019). From Molecular Machines to Stimuli-Responsive Materials. Adv. Mater. *32*, 1906036. https://doi.org/10.1002/adma.201906036.

76. Shklyaev, O.E., and Balazs, A.C. (2024). Interlinking spatial dimensions and kinetic processes in dissipative materials to create synthetic systems with lifelike functionality. Nat. Nanotechnol. *19*, 146–159. https://doi.org/10.1038/s41565-023-01530-z.

77. Zhou, H., Yamada, T., and Kimizuka, N. (2016). Supramolecular Thermo-Electrochemical Cells: Enhanced Thermoelectric Performance by Host-Guest Complexation and Salt-Induced Crystallization. J. Am. Chem. Soc. *138*, 10502–10507. https://doi.org/10.1021/jacs.6b04923.

78. Di Noja, S., Garrido, M., Gualandi, L., and Ragazzon, G. (2023). Control over Dethreading Kinetics Allows Evaluating the Entropy Stored in an Interlocked Molecular Machine Out-of-Equilibrium. Chem. Eur. J. *29*, e202300295. https://doi.org/10.1002/chem.202300295.

79. Tu, Y. (2008). The nonequilibrium mechanism for ultrasensitivity in a biological switch: Sensing by Maxwell's demons. Proc. Natl. Acad. Sci. USA *105*, 11737–11741. https://doi.org/10.1073/pnas.0804641105.

80. Krabbenborg, S.O., and Huskens, J. (2014). Electrochemically generated gradients. Angew. Chem. Int. Ed. *53*, 9152–9167. https://doi.org/10.1002/anie.201310349.

Chem, Volume *10*

Supplemental information

Analysis of kinetic asymmetry in a multi-cycle reaction network establishes the principles for autonomous compartmentalized molecular ratchets

Emanuele Penocchio, Ahmad Bachir, Alberto Credi, Raymond Dean Astumian, and Giulio Ragazzon

Supplemental Experimental Procedures

Contents

The Supporting Information is organized with the goal of analyzing the model network discussed in the main text, as an example of how kinetic asymmetry is calculated in multi-cycle networks.

S1 The model: assumptions and conventions

As discussed in the main text, we consider an electrochemical system subdivided into two compartments, I and II. All species can freely diffuse between the two compartments and each of the two compartments is well-mixed. In the compartment labelled "I", species are closer to electrode I kept at constant potential E_{I}. In the compartment labelled "II", species are closer to electrode II kept at constant potential E_{II}. This implies that species in compartment I (resp. II) can be oxidized or reduced by exchanging electrons with the electrode I (resp. II). The electrochemical potential gradient is defined as $\Delta E = E_{\mathrm{II}} - E_{\mathrm{I}}$, which is kept constant in experiments (no time-periodic driving). Finally, species can undergo chemical reactions, affording the compartmentalized reaction network depicted in Figure 1b of the main text. We are interested to identify the minimal requirements on the rate constants ks for generating kinetic asymmetry, *i.e.*, observing a preferred directionality of the chemical currents in the steady state. [S1] In particular, we want to investigate the implementation of an autonomous energy ratchet mechanism: namely, directionality is fully determined by the ratio of the equilibrium constants of the chemical reactions in the oxidized and reduced states. Therefore, in the following, we choose rate constants such that (i) they respect microscopic reversibility not to violate thermodynamic consistency, and (ii) the system is "as kinetically symmetric as possible", meaning that we will exclude any kinetic bias other than a difference in the chemical equilibria, when not otherwise stated.

S1.1 Electrochemical reactions

We model electrochemical reactions as first order unimolecular redox processes obeying Butler-Volmer kinetics: [S2]

$$\mathrm{A}_{\mathrm{ox}}^{(\mathrm{I})} \underset{k_{-1}}{\overset{k_{+1}}{\rightleftharpoons}} \mathrm{A}_{\mathrm{red}}^{(\mathrm{I})} \tag{1a}$$

$$\mathrm{B}_{\mathrm{ox}}^{(\mathrm{I})} \underset{k_{-2}}{\overset{k_{+2}}{\rightleftharpoons}} \mathrm{B}_{\mathrm{red}}^{(\mathrm{I})} \tag{1b}$$

$$\mathrm{A}_{\mathrm{ox}}^{(\mathrm{II})} \underset{k_{-3}}{\overset{k_{+3}}{\rightleftharpoons}} \mathrm{A}_{\mathrm{red}}^{(\mathrm{II})} \tag{1c}$$

$$\mathrm{B}_{\mathrm{ox}}^{(\mathrm{II})} \underset{k_{-4}}{\overset{k_{+4}}{\rightleftharpoons}} \mathrm{B}_{\mathrm{red}}^{(\mathrm{II})} \tag{1d}$$

As a convention, we consider the reduction as the forward process ($k_{+\mathrm{i}}$) and the oxidation as the backward process ($k_{-\mathrm{i}}$). The rate constants for a redox reaction i in the compartment x involving the chemical species σ take the following general form

$$k_{+\mathrm{i}} = k_{\mathrm{e,i}} e^{-\frac{\alpha_{\mathrm{i}} F}{RT}(E_{\mathrm{x}} - E^{\circ}_{\sigma})}\,; \quad k_{-\mathrm{i}} = k_{\mathrm{e,i}} e^{\frac{(1-\alpha_{\mathrm{i}}) F}{RT}(E_{\mathrm{x}} - E^{\circ}_{\sigma})} \tag{2}$$

where $k_{\mathrm{e,i}}$ is a frequency factor embedding all the kinetics features that determine the probability that the species σ interacts with the electrode x, α_{i} is the electrode charge transfer coefficient, E_{x} the potential at the electrode in compartment x, E°_{σ} the standard redox potential of species σ, F the Faraday constant, T the temperature, and R the universal gas constant.

In the following, we will assume that all the electrochemical processes have an electrode charge transfer coefficient $\alpha_{\mathrm{i}} = \alpha = 0.5$ (in accordance with previous modelling [S3]) and identical frequency factors $k_{\mathrm{e,i}} = k_{\mathrm{e}}$. In this way, we make sure that no kinetic bias (information ratchet effect) emerges from the electrochemical rates. Therefore, the electrochemical rate constants that we will consider in the following are:

$$k_{+1} = k_{\mathrm{e}} e^{-\Omega_{\mathrm{BV}}(E_{\mathrm{I}} - E^{\circ}_{\mathrm{A}})}\,; \quad k_{-1} = k_{\mathrm{e}} e^{+\Omega_{\mathrm{BV}}(E_{\mathrm{I}} - E^{\circ}_{\mathrm{A}})} \tag{3a}$$

$$k_{+2} = k_{\mathrm{e}} e^{-\Omega_{\mathrm{BV}}(E_{\mathrm{I}} - E^{\circ}_{\mathrm{B}})}\,; \quad k_{-2} = k_{\mathrm{e}} e^{+\Omega_{\mathrm{BV}}(E_{\mathrm{I}} - E^{\circ}_{\mathrm{B}})} \tag{3b}$$

$$k_{+3} = k_{\mathrm{e}} e^{-\Omega_{\mathrm{BV}}(E_{\mathrm{II}} - E^{\circ}_{\mathrm{A}})}\,; \quad k_{-3} = k_{\mathrm{e}} e^{+\Omega_{\mathrm{BV}}(E_{\mathrm{II}} - E^{\circ}_{\mathrm{A}})} \tag{3c}$$

$$k_{+4} = k_{\mathrm{e}} e^{-\Omega_{\mathrm{BV}}(E_{\mathrm{II}} - E^{\circ}_{\mathrm{B}})}\,; \quad k_{-4} = k_{\mathrm{e}} e^{+\Omega_{\mathrm{BV}}(E_{\mathrm{II}} - E^{\circ}_{\mathrm{B}})} \tag{3d}$$

where we defined $\Omega_{\mathrm{BV}} = F/2RT$.

S1.2 Chemical reactions

Chemical reactions are treated as first-order reactions:

$$\mathrm{B}^{(\mathrm{I})}_{\mathrm{red}} \underset{k_{-5}}{\overset{k_{+5}}{\rightleftharpoons}} \mathrm{A}^{(\mathrm{I})}_{\mathrm{red}} \tag{4a}$$

$$\mathrm{B}^{(\mathrm{I})}_{\mathrm{ox}} \underset{k_{-6}}{\overset{k_{+6}}{\rightleftharpoons}} \mathrm{A}^{(\mathrm{I})}_{\mathrm{ox}} \tag{4b}$$

$$\mathrm{B}^{(\mathrm{II})}_{\mathrm{red}} \underset{k_{-7}}{\overset{k_{+7}}{\rightleftharpoons}} \mathrm{A}^{(\mathrm{II})}_{\mathrm{red}} \tag{4c}$$

$$\mathrm{B}^{(\mathrm{II})}_{\mathrm{ox}} \underset{k_{-8}}{\overset{k_{+8}}{\rightleftharpoons}} \mathrm{A}^{(\mathrm{II})}_{\mathrm{ox}}\,. \tag{4d}$$

As a convention, we consider the reaction from B to A as the forward process ($k_{+\mathrm{i}}$) and the reaction from A to B as the backward process ($k_{-\mathrm{i}}$). Since we are interested in characterizing the system at the steady

state, we note that the same approach holds also for bimolecular reactions (e.g., the self-assembly of a dimer) treated as pseudo first-order processes.

In the following, we assume that the rate constants of the chemical reactions are not influenced by the compartment, thus excluding an information ratchet effect. Therefore:

$$k_{+5} = k_{+7} = k_{\mathrm{BA,red}}\,; \quad k_{-5} = k_{-7} = k_{\mathrm{AB,red}} \tag{5a}$$

$$k_{+6} = k_{+8} = k_{\mathrm{BA,ox}}\,; \quad k_{-6} = k_{-8} = k_{\mathrm{AB,ox}}\,. \tag{5b}$$

The corresponding equilibrium constants are defined as:

$$K_{\mathrm{red}} = \frac{k_{\mathrm{BA,red}}}{k_{\mathrm{AB,red}}}\,; \quad K_{\mathrm{ox}} = \frac{k_{\mathrm{BA,ox}}}{k_{\mathrm{AB,ox}}}\,. \tag{6}$$

S1.3 Diffusion

We treat diffusion as a set of additional reactions that model how species move from one compartment to the other:

$$\mathrm{A}_{\mathrm{ox}}^{(\mathrm{I})} \underset{k_{-9}}{\overset{k_{+9}}{\rightleftharpoons}} \mathrm{A}_{\mathrm{ox}}^{(\mathrm{II})} \tag{7a}$$

$$\mathrm{A}_{\mathrm{red}}^{(\mathrm{I})} \underset{k_{-10}}{\overset{k_{+10}}{\rightleftharpoons}} \mathrm{A}_{\mathrm{red}}^{(\mathrm{II})} \tag{7b}$$

$$\mathrm{B}_{\mathrm{ox}}^{(\mathrm{I})} \underset{k_{-11}}{\overset{k_{+11}}{\rightleftharpoons}} \mathrm{B}_{\mathrm{ox}}^{(\mathrm{II})} \tag{7c}$$

$$\mathrm{B}_{\mathrm{red}}^{(\mathrm{I})} \underset{k_{-12}}{\overset{k_{+12}}{\rightleftharpoons}} \mathrm{B}_{\mathrm{red}}^{(\mathrm{II})}\,. \tag{7d}$$

As a convention, we consider the diffusion from compartment I to compartment II as the forward process ($k_{+\mathrm{i}}$) and the diffusion from compartment II to compartment I as the backward process ($k_{-\mathrm{i}}$).

In the following, we will assume that there is no thermodynamic preference for a compartment with respect to the other, namely $k_{+\mathrm{i}} = k_{-\mathrm{i}}$. This assumption is justified by the presence, in the experimental setup [S3], of a supporting electrolyte in high concentration whose purpose is precisely inhibiting the species' preferred migration towards one of the electrodes, a common approach in electrochemical measurements [S2]. Furthermore, the diffusion rate constants of the species are reasonably assumed not to change under redox reactions [S4]. Finally, if not stated otherwise, we will consider the diffusion rate constants not to change upon chemical reactions. Therefore, when not otherwise stated, to exclude the possibility that a bias in the diffusion rate constants contributes to the directionality of the system, we consider all diffusion rate

constants as equal:

$$k_{\pm 9} = k_{\pm 10} = k_{\pm 11} = k_{\pm 12} = k_{\mathrm{d}} \,. \tag{8}$$

The effect of having diffusion asymmetry (*i.e.*, $k_{\pm 9} = k_{\pm 10} = k_{\mathrm{d,A}} \neq k_{\pm 11} = k_{\pm 12} = k_{\mathrm{d,B}}$) is discussed in Section S3.

S1.4 Thermodynamic consistency

Thermodynamic consistency imposes that, for any reaction cycle in the network that does not accomplish the net transport of an electron from an electrode to the other, the ratio between the product of the rate constants in the forward direction and in the backward direction must equal one. Within the above assumptions, the following condition guarantees the thermodynamic consistency of our model:

$$K_{\mathrm{ox}} K_{\mathrm{red}}^{-1} = e^{2\Omega_{\mathrm{BV}}(E_B^\circ - E_A^\circ)} = e^{2\Omega_{\mathrm{BV}} \Delta E^\circ} \,, \tag{9}$$

where we defined $\Delta E^\circ = E_B^\circ - E_A^\circ$.

S2 Trajectory thermodynamics analysis

In this Section, we explore analytically, using trajectory thermodynamics [S5–S7], whether it is possible to implement an autonomous energy ratchet mechanism in the network in Figure 1b of the main text within the assumptions specified in the previous section.

S2.1 Cycles classification and definition of directionality

To frame our question in the language of trajectory thermodynamics, it is useful to introduce some terminology.

In the presence of an electrochemical potential gradient $\Delta E > 0$, each cyclic sequence of chemical reactions realizing a net transport of electrons from the cathode to the anode, denoted here as a $\mathcal{C}$-cycle, will be travelled on average faster than its microscopic reverse $\mathcal{C}^\dagger$ at steady state:

$$\frac{j_{\mathcal{C}}}{j_{\mathcal{C}^\dagger}} = e^{2\Omega_{\mathrm{BV}}\Delta E}\,, \tag{10}$$

where $j_{\mathcal{C}}$ denotes the frequency (in units of time^{-1}) at which cycle $\mathcal{C}$ is travelled on average at steady state. Therefore, there will be a net, direct current of electrons from the cathode to the anode mediated by the system. Notice that, when the electrochemical potential gradient is null ($\Delta E = 0$), no preferred directionality emerges.

On the contrary, each cyclic sequence of chemical reactions that does not accomplish a net transport of electrons, denoted here as a $\mathcal{U}$-cycle, will always be travelled back and forth at the same average frequency as a consequence of microscopic reversibility:

$$\frac{j_{\mathcal{U}}}{j_{\mathcal{U}^\dagger}} = 1\,. \tag{11}$$

To establish whether the sequence S defined in the main text is more probable than the sequence S^{-1} (*i.e.*, whether there is directionality in the system), the first step is to identify all the cycles in the network realizing those sequences. To best organize the following derivations, we will divide the cycles in three categories. The forward cycles, $\mathcal{F}$, are those $\mathcal{C}$-cycles that realize the sequence S and concomitantly move one electron from the cathode to the anode. The backward cycles, $\mathcal{B}$, are those $\mathcal{C}$-cycles that realize the sequence S^{-1} and concomitantly move one electrode from the cathode to the anode. The slip cycles, $\mathcal{R}$, are those $\mathcal{U}$-cycles realizing the sequence S without moving any net number of electrons from cathode to anode.

Mathematically, K_r (as defined in the main text) can be computed by dividing the sum of the frequencies ($j_{\mathcal{X}}$) of all the cycles realizing the sequence $\mathcal{S}$ by the sum of the frequencies of all the cycles realizing the

sequence $\mathcal{S}^{-1}$:

$$K_r = \frac{f(\mathrm{S})}{f(\mathrm{S}^{-1})} = \frac{\sum_i j_{\mathcal{F}_i} + \sum_i j_{\mathcal{B}_i^\dagger} + \sum_i j_{\mathcal{R}_i}}{\sum_i j_{\mathcal{F}_i^\dagger} + \sum_i j_{\mathcal{B}_i} + \sum_i j_{\mathcal{R}_i^\dagger}}\,, \tag{12}$$

where summations are intended to run over all the forward, backward, and slip cycles. By implementing microscopic reversibility, *i.e.*, Equations (10) and (11), Equation (12) can be simplified to:

$$\begin{aligned} K_r =& \frac{\sum_i j_{\mathcal{F}_i} + e^{-2\Omega_{\mathrm{BV}}\Delta E}\sum_i j_{\mathcal{B}_i} + \sum_i j_{\mathcal{R}_i}}{e^{-2\Omega_{\mathrm{BV}}\Delta E}\sum_i j_{\mathcal{F}_i} + \sum_i j_{\mathcal{B}_i} + \sum_i j_{\mathcal{R}_i}} \\ =& \frac{q + e^{-2\Omega_{\mathrm{BV}}\Delta E} + \Gamma}{q e^{-2\Omega_{\mathrm{BV}}\Delta E} + 1 + \Gamma} \\ \text{with} \quad q =& \frac{\sum_i j_{\mathcal{F}_i}}{\sum_i j_{\mathcal{B}_i}}\,, \quad \text{and} \quad \Gamma = \frac{\sum_i j_{\mathcal{R}_i}}{\sum_i j_{\mathcal{B}_i}}\,. \end{aligned} \tag{13}$$

Equation (13) shows that three parameters, ΔE, q, and Γ fully determine directionality. To better understand the role of each of them, it is instructive to take the difference between the numerator (num) and denominator (dem) of the fraction in Equation (13):

$$\mathrm{num} - \mathrm{dem} = q + e^{-2\Omega_{\mathrm{BV}}\Delta E} + \Gamma - q e^{-2\Omega_{\mathrm{BV}}\Delta E} - 1 - \Gamma = (1 - e^{-2\Omega_{\mathrm{BV}}\Delta E}) \times (q - 1)\,. \tag{14}$$

The above expression stresses that, when $\Delta E > 0$ (and therefore $1 - e^{-2\Omega_{\mathrm{BV}}\Delta E} > 0$), K_r will be greater (smaller) than one if $q > (<)1$, since the numerator of the fraction in Equation (13) will be larger (smaller) than the denominator. On the contrary, when $\Delta E < 0$ (and therefore $1 - e^{-2\Omega_{\mathrm{BV}}\Delta E} < 0$), K_r will be greater (smaller) than one if $q < (>)1$. If $\Delta E = 0$ and/or $q = 1$, $K_r = 1$ (no directionality), showing that the presence of a thermodynamic driving force ($\Delta E \neq 0$) and an overall kinetic bias ($q \neq 1$) are both necessary to generate directionality.

S2.2 Diagram method for cycle frequencies

The relevant cycles to consider for establishing whether or not directionality emerges in the system are depicted in Figure 2 of the main text. There are four forward cycles and four backward cycles. Therefore, the quantity of interest is:

$$q = \frac{\sum_i j_{\mathcal{F}_i}}{\sum_i j_{\mathcal{B}_i}} = \frac{j_{\mathcal{F}_1} + j_{\mathcal{F}_2} + j_{\mathcal{F}_3} + j_{\mathcal{F}_4}}{j_{\mathcal{B}_1} + j_{\mathcal{B}_2} + j_{\mathcal{B}_3} + j_{\mathcal{B}_4}}\,. \tag{15}$$

To proceed, the next step is to compute all the eight $j_{\mathcal{X}}$s appearing in the quantity above. To do that, we will use the diagram method illustrated in Ref. [S8]. We anticipate that the frequences can be expressed in the following form:

$$j_{\mathcal{X}} = \frac{\Pi_{\mathcal{X}} \Sigma_{\mathcal{X}}}{N}\,. \tag{16}$$

In the following Section, we discuss in details how $\Pi_{\mathcal{X}}$ and $\Sigma_{\mathcal{X}}$ can be expressed for a given cycle. Notice that computing the normalizing constant is not necessary, as Equation (15) boils down to:

$$q = \frac{\Pi_{\mathcal{F}_1}\Sigma_{\mathcal{F}_1} + \Pi_{\mathcal{F}_2}\Sigma_{\mathcal{F}_2} + \Pi_{\mathcal{F}_3}\Sigma_{\mathcal{F}_3} + \Pi_{\mathcal{F}_4}\Sigma_{\mathcal{F}_4}}{\Pi_{\mathcal{B}_1}\Sigma_{\mathcal{B}_1} + \Pi_{\mathcal{B}_2}\Sigma_{\mathcal{B}_2} + \Pi_{\mathcal{B}_3}\Sigma_{\mathcal{B}_3} + \Pi_{\mathcal{B}_4}\Sigma_{\mathcal{B}_4}}\,. \tag{17}$$

S2.2.1 A detailed example: computing $\Sigma_{\mathcal{F}_1}$ and $\Pi_{\mathcal{F}_1}$ graphically

In this Section, we explain how $\Sigma_{\mathcal{F}_1}$ and $\Pi_{\mathcal{F}_1}$ can be computed for the cycle $\mathcal{F}_1$ (see Figure 2 in the main text). The term $\Pi_{\mathcal{F}_1}$ is the product of all the rate constants involved in the cycle:

$$\Pi_{\mathcal{F}_1} = k_{\mathrm{e}} e^{-\Omega_{\mathrm{BV}}(E_{\mathrm{I}} - E^{\circ}_{\mathrm{A}})} \times k_{\mathrm{AB,red}} \times k_{\mathrm{d}} \times k_{\mathrm{e}} e^{+\Omega_{\mathrm{BV}}(E_{\mathrm{II}} - E^{\circ}_{\mathrm{B}})} \times k_{\mathrm{BA,ox}} \times k_{\mathrm{d}}\,. \tag{18}$$

The term $\Sigma_{\mathcal{F}_1}$ is the sum of the contributions from all the so-called "rooted spanning trees" [S9] of cycle $\mathcal{F}_1$. A rooted spanning tree is a sequence of reactions entering the cycle starting from all the states not included in the cycle and without forming new cycles. All the rooted spanning trees of cycle $\mathcal{F}_1$ are depicted in Figure 3 of the main text. The contribution to $\Sigma_{\mathcal{F}_1}$ of each spanning tree is the product of the rate constants involved. Therefore:

$$\begin{aligned}
\Sigma_{\mathcal{F}_1} =& k_{\mathrm{BA,ox}} \times k_{\mathrm{AB,red}} + k_{\mathrm{BA,ox}} \times k_{\mathrm{e}} e^{+\Omega_{\mathrm{BV}}(E_{\mathrm{II}} - E^{\circ}_{\mathrm{A}})} + k_{\mathrm{BA,ox}} \times k_{\mathrm{d}} \\
&+ k_{\mathrm{e}} e^{-\Omega_{\mathrm{BV}}(E_{\mathrm{I}} - E^{\circ}_{\mathrm{B}})} \times k_{\mathrm{AB,red}} + k_{\mathrm{e}} e^{-\Omega_{\mathrm{BV}}(E_{\mathrm{I}} - E^{\circ}_{\mathrm{B}})} \times k_{\mathrm{e}} e^{+\Omega_{\mathrm{BV}}(E_{\mathrm{II}} - E^{\circ}_{\mathrm{A}})} + k_{\mathrm{e}} e^{-\Omega_{\mathrm{BV}}(E_{\mathrm{I}} - E^{\circ}_{\mathrm{B}})} \times k_{\mathrm{d}} \\
&+ k_{\mathrm{d}} \times k_{\mathrm{AB,red}} + k_{\mathrm{d}} \times k_{\mathrm{e}} e^{+\Omega_{\mathrm{BV}}(E_{\mathrm{II}} - E^{\circ}_{\mathrm{A}})} + k_{\mathrm{d}} \times k_{\mathrm{d}} = \\
=& \left(k_{\mathrm{BA,ox}} + k_{\mathrm{e}} e^{-\Omega_{\mathrm{BV}}(E_{\mathrm{I}} - E^{\circ}_{\mathrm{B}})} + k_{\mathrm{d}}\right) \times \left(k_{\mathrm{AB,red}} + k_{\mathrm{e}} e^{+\Omega_{\mathrm{BV}}(E_{\mathrm{II}} - E^{\circ}_{\mathrm{A}})} + k_{\mathrm{d}}\right)
\end{aligned} \tag{19}$$

S2.2.2 All cycle frequencies

Here, we list the terms $\Pi_{\mathcal{X}}$ and $\Sigma_{\mathcal{X}}$ for all the cycles, computed as described in the previous Section.

For cycle $\mathcal{F}_1$:

$$\Pi_{\mathcal{F}_1} = k_{\mathrm{e}} e^{-\Omega_{\mathrm{BV}}(E_{\mathrm{I}} - E^{\circ}_{\mathrm{A}})} \times k_{\mathrm{AB,red}} \times k_{\mathrm{d}} \times k_{\mathrm{e}} e^{+\Omega_{\mathrm{BV}}(E_{\mathrm{II}} - E^{\circ}_{\mathrm{B}})} \times k_{\mathrm{BA,ox}} \times k_{\mathrm{d}} \tag{20a}$$

$$\Sigma_{\mathcal{F}_1} = \left(k_{\mathrm{BA,ox}} + k_{\mathrm{e}} e^{-\Omega_{\mathrm{BV}}(E_{\mathrm{I}} - E^{\circ}_{\mathrm{B}})} + k_{\mathrm{d}}\right) \times \left(k_{\mathrm{AB,red}} + k_{\mathrm{e}} e^{+\Omega_{\mathrm{BV}}(E_{\mathrm{II}} - E^{\circ}_{\mathrm{A}})} + k_{\mathrm{d}}\right) \tag{20b}$$

For cycle $\mathcal{F}_2$:

$$\Pi_{\mathcal{F}_2} = k_\mathrm{e} e^{-\Omega_\mathrm{BV}(E_\mathrm{I} - E_\mathrm{A}^\circ)} \times k_\mathrm{d} \times k_\mathrm{AB,red} \times k_\mathrm{e} e^{+\Omega_\mathrm{BV}(E_\mathrm{II} - E_\mathrm{B}^\circ)} \times k_\mathrm{BA,ox} \times k_\mathrm{d} \tag{21a}$$

$$\Sigma_{\mathcal{F}_2} = (k_\mathrm{BA,ox} + k_\mathrm{d}) \times \left(k_\mathrm{BA,red} + k_\mathrm{e} e^{+\Omega_\mathrm{BV}(E_\mathrm{I} - E_\mathrm{B}^\circ)} + k_\mathrm{d}\right) + k_\mathrm{e} e^{-\Omega_\mathrm{BV}(E_\mathrm{I} - E_\mathrm{B}^\circ)} \times (k_\mathrm{BA,red} + k_\mathrm{d}) \tag{21b}$$

For cycle $\mathcal{F}_3$:

$$\Pi_{\mathcal{F}_3} = k_\mathrm{e} e^{-\Omega_\mathrm{BV}(E_\mathrm{I} - E_\mathrm{A}^\circ)} \times k_\mathrm{d} \times k_\mathrm{AB,red} \times k_\mathrm{e} e^{+\Omega_\mathrm{BV}(E_\mathrm{II} - E_\mathrm{B}^\circ)} \times k_\mathrm{d} \times k_\mathrm{BA,ox} \tag{22a}$$

$$\Sigma_{\mathcal{F}_3} = \left(k_\mathrm{BA,red} + k_\mathrm{e} e^{+\Omega_\mathrm{BV}(E_\mathrm{I} - E_\mathrm{B}^\circ)} + k_\mathrm{d}\right) \times \left(k_\mathrm{AB,ox} + k_\mathrm{e} e^{-\Omega_\mathrm{BV}(E_\mathrm{II} - E_\mathrm{A}^\circ)} + k_\mathrm{d}\right) \tag{22b}$$

For cycle $\mathcal{F}_4$:

$$\Pi_{\mathcal{F}_4} = k_\mathrm{e} e^{-\Omega_\mathrm{BV}(E_\mathrm{I} - E_\mathrm{A}^\circ)} \times k_\mathrm{AB,red} \times k_\mathrm{d} \times k_\mathrm{e} e^{+\Omega_\mathrm{BV}(E_\mathrm{II} - E_\mathrm{B}^\circ)} \times k_\mathrm{d} \times k_\mathrm{BA,ox} \tag{23a}$$

$$\Sigma_{\mathcal{F}_4} = (k_\mathrm{AB,ox} + k_\mathrm{d}) \times \left(k_\mathrm{AB,red} + k_\mathrm{e} e^{+\Omega_\mathrm{BV}(E_\mathrm{II} - E_\mathrm{A}^\circ)} + k_\mathrm{d}\right) + k_\mathrm{e} e^{-\Omega_\mathrm{BV}(E_\mathrm{II} - E_\mathrm{A}^\circ)} \times (k_\mathrm{AB,red} + k_\mathrm{d}) \tag{23b}$$

For cycle $\mathcal{B}_1$:

$$\Pi_{\mathcal{B}_1} = k_\mathrm{e} e^{-\Omega_\mathrm{BV}(E_\mathrm{I} - E_\mathrm{B}^\circ)} \times k_\mathrm{BA,red} \times k_\mathrm{d} \times k_\mathrm{e} e^{+\Omega_\mathrm{BV}(E_\mathrm{II} - E_\mathrm{A}^\circ)} \times k_\mathrm{AB,ox} \times k_\mathrm{d} \tag{24a}$$

$$\Sigma_{\mathcal{B}_1} = \left(k_\mathrm{AB,ox} + k_\mathrm{e} e^{-\Omega_\mathrm{BV}(E_\mathrm{I} - E_\mathrm{A}^\circ)} + k_\mathrm{d}\right) \times \left(k_\mathrm{BA,red} + k_\mathrm{e} e^{+\Omega_\mathrm{BV}(E_\mathrm{II} - E_\mathrm{B}^\circ)} + k_\mathrm{d}\right) \tag{24b}$$

For cycle $\mathcal{B}_2$:

$$\Pi_{\mathcal{B}_2} = k_\mathrm{e} e^{-\Omega_\mathrm{BV}(E_\mathrm{I} - E_\mathrm{B}^\circ)} \times k_\mathrm{d} \times k_\mathrm{BA,red} \times k_\mathrm{e} e^{+\Omega_\mathrm{BV}(E_\mathrm{II} - E_\mathrm{A}^\circ)} \times k_\mathrm{AB,ox} \times k_\mathrm{d} \tag{25a}$$

$$\Sigma_{\mathcal{B}_2} = (k_\mathrm{AB,ox} + k_\mathrm{d}) \times \left(k_\mathrm{AB,red} + k_\mathrm{e} e^{+\Omega_\mathrm{BV}(E_\mathrm{I} - E_\mathrm{A}^\circ)} + k_\mathrm{d}\right) + k_\mathrm{e} e^{-\Omega_\mathrm{BV}(E_\mathrm{I} - E_\mathrm{A}^\circ)} (k_\mathrm{AB,red} + k_\mathrm{d}) \tag{25b}$$

For cycle $\mathcal{B}_3$:

$$\Pi_{\mathcal{B}_3} = k_{\mathrm{e}} e^{-\Omega_{\mathrm{BV}}(E_{\mathrm{I}} - E^{\circ}_{\mathrm{B}})} \times k_{\mathrm{d}} \times k_{\mathrm{BA,red}} \times k_{\mathrm{e}} e^{+\Omega_{\mathrm{BV}}(E_{\mathrm{II}} - E^{\circ}_{\mathrm{A}})} \times k_{\mathrm{d}} \times k_{\mathrm{AB,ox}} \tag{26a}$$

$$\Sigma_{\mathcal{B}_3} = \left(k_{\mathrm{AB,red}} + k_{\mathrm{e}} e^{+\Omega_{\mathrm{BV}}(E_{\mathrm{I}} - E^{\circ}_{\mathrm{A}})} + k_{\mathrm{d}}\right) \times \left(k_{\mathrm{BA,ox}} + k_{\mathrm{e}} e^{-\Omega_{\mathrm{BV}}(E_{\mathrm{II}} - E^{\circ}_{\mathrm{B}})} + k_{\mathrm{d}}\right) \tag{26b}$$

For cycle $\mathcal{B}_4$:

$$\Pi_{\mathcal{B}_4} = k_{\mathrm{e}} e^{-\Omega_{\mathrm{BV}}(E_{\mathrm{I}} - E^{\circ}_{\mathrm{B}})} \times k_{\mathrm{BA,red}} \times k_{\mathrm{d}} \times k_{\mathrm{e}} e^{+\Omega_{\mathrm{BV}}(E_{\mathrm{II}} - E^{\circ}_{\mathrm{A}})} \times k_{\mathrm{d}} \times k_{\mathrm{AB,ox}} \tag{27a}$$

$$\Sigma_{\mathcal{B}_4} = (k_{\mathrm{BA,ox}} + k_{\mathrm{d}}) \times \left(k_{\mathrm{BA,red}} + k_{\mathrm{e}} e^{+\Omega_{\mathrm{BV}}(E_{\mathrm{II}} - E^{\circ}_{\mathrm{B}})} + k_{\mathrm{d}}\right) + k_{\mathrm{e}} e^{-\Omega_{\mathrm{BV}}(E_{\mathrm{II}} - E^{\circ}_{\mathrm{B}})} (k_{\mathrm{BA,red}} + k_{\mathrm{d}}) \tag{27b}$$

S2.2.3 Computation of q

We notice that $\Pi_{\mathcal{F}_1} = \Pi_{\mathcal{F}_2} = \Pi_{\mathcal{F}_3} = \Pi_{\mathcal{F}_4} := \Pi_{\mathcal{F}}$ and $\Pi_{\mathcal{B}_1} = \Pi_{\mathcal{B}_2} = \Pi_{\mathcal{B}_3} = \Pi_{\mathcal{B}_4} := \Pi_{\mathcal{B}}$. Furthermore, by using Equation 9:

$$\frac{\Pi_{\mathcal{F}}}{\Pi_{\mathcal{B}}} = \frac{k_{\mathrm{e}} e^{-\Omega_{\mathrm{BV}}(E_{\mathrm{I}} - E^{\circ}_{\mathrm{A}})} \times k_{\mathrm{AB,red}} \times k_{\mathrm{e}} e^{+\Omega_{\mathrm{BV}}(E_{\mathrm{II}} - E^{\circ}_{\mathrm{B}})} \times k_{\mathrm{BA,ox}}}{k_{\mathrm{e}} e^{-\Omega_{\mathrm{BV}}(E_{\mathrm{I}} - E^{\circ}_{\mathrm{B}})} \times k_{\mathrm{BA,red}} \times k_{\mathrm{e}} e^{+\Omega_{\mathrm{BV}}(E_{\mathrm{II}} - E^{\circ}_{\mathrm{A}})} \times k_{\mathrm{AB,ox}}} = e^{-2\Omega_{\mathrm{BV}} \Delta E^{\circ}} \times K_{\mathrm{ox}} \times K_{\mathrm{red}}^{-1} = 1\,. \tag{28}$$

As a consequence, Equation (17) boils down to:

$$q = \frac{\Sigma_{\mathcal{F}_1} + \Sigma_{\mathcal{F}_2} + \Sigma_{\mathcal{F}_3} + \Sigma_{\mathcal{F}_4}}{\Sigma_{\mathcal{B}_1} + \Sigma_{\mathcal{B}_2} + \Sigma_{\mathcal{B}_3} + \Sigma_{\mathcal{B}_4}}\,. \tag{29}$$

Therefore, to compute q, we need to evaluate the following sums:

$$\begin{aligned}
\Sigma_{\mathcal{F}_1} + \Sigma_{\mathcal{F}_2} + \Sigma_{\mathcal{F}_3} + \Sigma_{\mathcal{F}_4} = {} & (k_{\mathrm{BA,ox}} + k_{\mathrm{AB,ox}} + 2k_{\mathrm{d}}) \times \left(k_{\mathrm{e}} e^{+\Omega_{\mathrm{BV}}(E_{\mathrm{I}} - E^{\circ}_{\mathrm{B}})} + k_{\mathrm{e}} e^{+\Omega_{\mathrm{BV}}(E_{\mathrm{II}} - E^{\circ}_{\mathrm{A}})}\right) + \\
& (k_{\mathrm{BA,red}} + k_{\mathrm{AB,red}} + 2k_{\mathrm{d}}) \times \left(k_{\mathrm{e}} e^{-\Omega_{\mathrm{BV}}(E_{\mathrm{I}} - E^{\circ}_{\mathrm{B}})} + k_{\mathrm{e}} e^{-\Omega_{\mathrm{BV}}(E_{\mathrm{II}} - E^{\circ}_{\mathrm{A}})}\right) + \\
& \left(k_{\mathrm{e}} e^{-\Omega_{\mathrm{BV}}(E_{\mathrm{I}} - E^{\circ}_{\mathrm{B}})} \times k_{\mathrm{e}} e^{+\Omega_{\mathrm{BV}}(E_{\mathrm{II}} - E^{\circ}_{\mathrm{A}})} + k_{\mathrm{e}} e^{+\Omega_{\mathrm{BV}}(E_{\mathrm{I}} - E^{\circ}_{\mathrm{B}})} \times k_{\mathrm{e}} e^{-\Omega_{\mathrm{BV}}(E_{\mathrm{II}} - E^{\circ}_{\mathrm{A}})}\right) + \\
& (k_{\mathrm{BA,ox}} + k_{\mathrm{AB,ox}} + 2k_{\mathrm{d}}) \times (k_{\mathrm{BA,red}} + k_{\mathrm{AB,red}} + 2k_{\mathrm{d}}) = \\
= {} & \left(e^{\Omega_{\mathrm{BV}} \Delta E} e^{\Omega_{\mathrm{BV}} \Delta E^{\circ}} + 1\right) \times C_1 + \left(e^{2\Omega_{\mathrm{BV}} \Delta E} e^{2\Omega_{\mathrm{BV}} \Delta E^{\circ}} + 1\right) \times C_2 + C_3
\end{aligned} \tag{30}$$

$$\begin{aligned}\Sigma_{\mathcal{B}_1}+\Sigma_{\mathcal{B}_2}+\Sigma_{\mathcal{B}_3}+\Sigma_{\mathcal{B}_4} &= (k_{\mathrm{BA,ox}}+k_{\mathrm{AB,ox}}+2k_{\mathrm{d}})\times\left(k_{\mathrm{e}}e^{+\Omega_{\mathrm{BV}}(E_{\mathrm{I}}-E^{\circ}_{\mathrm{A}})}+k_{\mathrm{e}}e^{+\Omega_{\mathrm{BV}}(E_{\mathrm{II}}-E^{\circ}_{\mathrm{B}})}\right)+\\ &\quad (k_{\mathrm{BA,red}}+k_{\mathrm{AB,red}}+2k_{\mathrm{d}})\times\left(k_{\mathrm{e}}e^{-\Omega_{\mathrm{BV}}(E_{\mathrm{I}}-E^{\circ}_{\mathrm{A}})}+k_{\mathrm{e}}e^{-\Omega_{\mathrm{BV}}(E_{\mathrm{II}}-E^{\circ}_{\mathrm{B}})}\right)+\\ &\quad \left(k_{\mathrm{e}}e^{+\Omega_{\mathrm{BV}}(E_{\mathrm{I}}-E^{\circ}_{\mathrm{A}})}\times k_{\mathrm{e}}e^{-\Omega_{\mathrm{BV}}(E_{\mathrm{II}}-E^{\circ}_{\mathrm{B}})}+k_{\mathrm{e}}e^{-\Omega_{\mathrm{BV}}(E_{\mathrm{I}}-E^{\circ}_{\mathrm{A}})}\times k_{\mathrm{e}}e^{+\Omega_{\mathrm{BV}}(E_{\mathrm{II}}-E^{\circ}_{\mathrm{B}})}\right)+\\ &\quad (k_{\mathrm{BA,ox}}+k_{\mathrm{AB,ox}}+2k_{\mathrm{d}})\times(k_{\mathrm{BA,red}}+k_{\mathrm{AB,red}}+2k_{\mathrm{d}})=\\ &= \left(e^{\Omega_{\mathrm{BV}}\Delta E}+e^{\Omega_{\mathrm{BV}}\Delta E^{\circ}}\right)\times C_1+\left(e^{2\Omega_{\mathrm{BV}}\Delta E}+e^{2\Omega_{\mathrm{BV}}\Delta E^{\circ}}\right)\times C_2+C_3 \end{aligned} \tag{31}$$

where

$$C_1 = (k_{\mathrm{BA,ox}}+k_{\mathrm{AB,ox}}+2k_{\mathrm{d}})\times k_{\mathrm{e}}e^{+\Omega_{\mathrm{BV}}(E_{\mathrm{I}}-E^{\circ}_{\mathrm{B}})}+(k_{\mathrm{BA,red}}+k_{\mathrm{AB,red}}+2k_{\mathrm{d}})\times k_{\mathrm{e}}e^{-\Omega_{\mathrm{BV}}(E_{\mathrm{II}}-E^{\circ}_{\mathrm{A}})} \tag{32}$$

$$C_2 = k_e^2 e^{-\Omega_{\mathrm{BV}}(\Delta E+\Delta E^{\circ})} \tag{33}$$

$$C_3 = (k_{\mathrm{BA,ox}}+k_{\mathrm{AB,ox}}+2k_{\mathrm{d}})\times(k_{\mathrm{BA,red}}+k_{\mathrm{AB,red}}+2k_{\mathrm{d}})\ . \tag{34}$$

Given the final form of Equations (30) and (31), we conclude that the ratio q in Equation (29) will be larger than, smaller than, or equal to one depending on whether the following fractions are larger than, smaller than, or equal to one:

$$\frac{e^{\Omega_{\mathrm{BV}}\Delta E}e^{\Omega_{\mathrm{BV}}\Delta E^{\circ}}+1}{e^{\Omega_{\mathrm{BV}}\Delta E}+e^{\Omega_{\mathrm{BV}}\Delta E^{\circ}}}\ ,\quad \frac{e^{2\Omega_{\mathrm{BV}}\Delta E}e^{2\Omega_{\mathrm{BV}}\Delta E^{\circ}}+1}{e^{2\Omega_{\mathrm{BV}}\Delta E}+e^{2\Omega_{\mathrm{BV}}\Delta E^{\circ}}} \tag{35}$$

As we explicitly prove in the next Section S2.2.4, this means that q is completely controlled by the sign of $\Delta E\Delta E^{\circ}$, *i.e.*, $q>1$ if $\Delta E\Delta E^{\circ}>0$,$q<1$ if $\Delta E\Delta E^{\circ}<0$, and $q=1$ (no directionality) if $\Delta E\Delta E^{\circ}=0$.

S2.2.4 Useful Mathematical Fact

Here, we explicitly justify the final conclusion of the previous Section, *i.e.*, q is controlled by the sign of the factor $\Delta E\Delta E^{\circ}$. To see that mathematically, consider any two positive numbers $A=1+\delta_A$ and $B=1+\delta_B$, where the signs of δ_A and δ_B control whether A and B are, respectively, larger than, smaller than, or equal to one. As a consequence, any fraction of the kind

$$\frac{AB+1}{A+B}=\frac{2+\delta_A+\delta_B+\delta_A\delta_B}{2+\delta_A+\delta_B} \tag{36}$$

will be larger that one if $\delta_A\delta_B > 0$ (A and B both larger or smaller than one), smaller than one if $\delta_A\delta_B < 0$ ($A > 1$ and $B < 1$ or vice-versa), and equal to one if $\delta_A\delta_B = 0$ (A and/or B equal to one). The fractions in Equation (34) are of the kind of the one in Equation (36). Indeed, $e^{\Omega_{\rm BV}\Delta E}$, $e^{\Omega_{\rm BV}\Delta E^\circ}$, $e^{2\Omega_{\rm BV}\Delta E}$, and $e^{2\Omega_{\rm BV}\Delta E^\circ}$ are all positive numbers being larger than, smaller than, or equal to one depending on the sign of ΔE and ΔE°.

S2.3 The nonequilibrium pumping equation

The diagrammatic methods illustrated in the previous Section can also be used to evaluate analytically the effect of kinetic asymmetry on concentrations ratios. Here, we evaluate whether the following steady state ratios

$$\frac{[\mathrm{A}^{(\mathrm{I})}_{\mathrm{ox}}]_{\mathrm{ss}} + [\mathrm{A}^{(\mathrm{II})}_{\mathrm{ox}}]_{\mathrm{ss}}}{[\mathrm{B}^{(\mathrm{I})}_{\mathrm{ox}}]_{\mathrm{ss}} + [\mathrm{B}^{(\mathrm{II})}_{\mathrm{ox}}]_{\mathrm{ss}}} \,, \quad \frac{[\mathrm{A}^{(\mathrm{I})}_{\mathrm{red}}]_{\mathrm{ss}} + [\mathrm{A}^{(\mathrm{II})}_{\mathrm{red}}]_{\mathrm{ss}}}{[\mathrm{B}^{(\mathrm{I})}_{\mathrm{red}}]_{\mathrm{ss}} + [\mathrm{B}^{(\mathrm{II})}_{\mathrm{red}}]_{\mathrm{ss}}} \tag{37}$$

are larger, smaller, or equal to the corresponding equilibrium ratios

$$\frac{[\mathrm{A}^{(\mathrm{I})}_{\mathrm{ox}}]_{\mathrm{eq}} + [\mathrm{A}^{(\mathrm{II})}_{\mathrm{ox}}]_{\mathrm{eq}}}{[\mathrm{B}^{(\mathrm{I})}_{\mathrm{ox}}]_{\mathrm{eq}} + [\mathrm{B}^{(\mathrm{II})}_{\mathrm{ox}}]_{\mathrm{eq}}} = K_{\mathrm{ox}} \,, \quad \frac{[\mathrm{A}^{(\mathrm{I})}_{\mathrm{red}}]_{\mathrm{eq}} + [\mathrm{A}^{(\mathrm{II})}_{\mathrm{red}}]_{\mathrm{eq}}}{[\mathrm{B}^{(\mathrm{I})}_{\mathrm{red}}]_{\mathrm{eq}} + [\mathrm{B}^{(\mathrm{II})}_{\mathrm{red}}]_{\mathrm{eq}}} = K_{\mathrm{red}} \,. \tag{38}$$

To do so, we leverage the expression of steady state concentrations $[X]_{\mathrm{ss}}$ in terms of the spanning trees of the graph representing the chemical reaction network rooted in the vertex corresponding to species X [S8–S11]:

$$[X]_{\mathrm{ss}} = \frac{1}{N}\sum_i \mathcal{T}_i^X \,, \tag{39}$$

where the summation runs over all the spanning trees rooted in X and $\mathcal{T}_i^X$ is the product of all the kinetic rate constants associated to the oriented edges in the spanning tree i. In the following Section, we discuss an example showing how to express the steady state concentration of a given species in terms of its $\mathcal{T}_i^X$ terms. Notice that computing the normalizing constant N is not necessary, as the ratios in (37) boil down to:

$$\frac{[\mathrm{A}^{(\mathrm{I})}_{\mathrm{ox}}]_{\mathrm{ss}} + [\mathrm{A}^{(\mathrm{II})}_{\mathrm{ox}}]_{\mathrm{ss}}}{[\mathrm{B}^{(\mathrm{I})}_{\mathrm{ox}}]_{\mathrm{ss}} + [\mathrm{B}^{(\mathrm{II})}_{\mathrm{ox}}]_{\mathrm{ss}}} = \frac{\sum_i \mathcal{T}_i^{\mathrm{A}^{(\mathrm{I})}_{\mathrm{ox}}} + \sum_i \mathcal{T}_i^{\mathrm{A}^{(\mathrm{II})}_{\mathrm{ox}}}}{\sum_i \mathcal{T}_i^{\mathrm{B}^{(\mathrm{I})}_{\mathrm{ox}}} + \sum_i \mathcal{T}_i^{\mathrm{B}^{(\mathrm{II})}_{\mathrm{ox}}}} \,, \quad \frac{[\mathrm{A}^{(\mathrm{I})}_{\mathrm{red}}]_{\mathrm{ss}} + [\mathrm{A}^{(\mathrm{II})}_{\mathrm{red}}]_{\mathrm{ss}}}{[\mathrm{B}^{(\mathrm{I})}_{\mathrm{red}}]_{\mathrm{ss}} + [\mathrm{B}^{(\mathrm{II})}_{\mathrm{red}}]_{\mathrm{ss}}} = \frac{\sum_i \mathcal{T}_i^{\mathrm{A}^{(\mathrm{I})}_{\mathrm{red}}} + \sum_i \mathcal{T}_i^{\mathrm{A}^{(\mathrm{II})}_{\mathrm{red}}}}{\sum_i \mathcal{T}_i^{\mathrm{B}^{(\mathrm{I})}_{\mathrm{red}}} + \sum_i \mathcal{T}_i^{\mathrm{B}^{(\mathrm{II})}_{\mathrm{red}}}} \,. \tag{40}$$

S2.3.1 A detailed example: expressing $[\mathrm{A}^{(\mathrm{I})}_{\mathrm{ox}}]_{\mathrm{ss}}$ in terms of $\mathcal{T}_i^{\mathrm{A}^{(\mathrm{I})}_{\mathrm{ox}}}$

A rooted spanning tree associated to a particular species in the chemical reaction network is a spanning tree with its edges oriented such that all edges point towards the root. Two exemplar spanning trees rooted in species $\mathrm{A}^{(\mathrm{I})}_{\mathrm{ox}}$ are represented in Figure S1a and b. Finding all the spanning trees associated to a given species might be challenging for large networks. However, we can still use Equation (39) and trajectory

thermodynamics to derive useful analytical expressions.

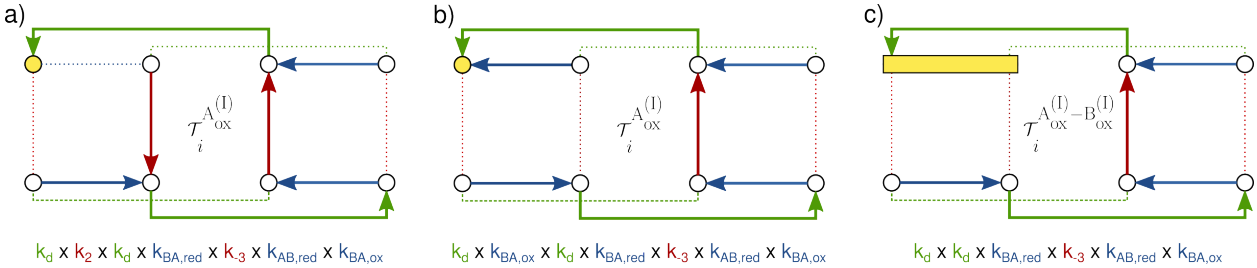

Figure S1: Exemplar spanning trees and corresponding $\mathcal{T}_i^{\mathcal{X}}$ terms. The network species, reactions, and color-coding coincide with those reported in Figure 1b and 2 in the main text. a) A spanning tree rooted in species $\mathrm{A}_{\mathrm{ox}}^{(\mathrm{I})}$ that does not contain the edge $\mathrm{B}_{\mathrm{ox}}^{(\mathrm{I})} \to \mathrm{A}_{\mathrm{ox}}^{(\mathrm{I})}$. b) A spanning tree rooted in species $\mathrm{A}_{\mathrm{ox}}^{(\mathrm{I})}$ that contains the edge $\mathrm{B}_{\mathrm{ox}}^{(\mathrm{I})} \to \mathrm{A}_{\mathrm{ox}}^{(\mathrm{I})}$. c) A spanning tree rooted in the edge $\mathrm{A}_{\mathrm{ox}}^{(\mathrm{I})} - \mathrm{B}_{\mathrm{ox}}^{(\mathrm{I})}$.

To proceed, we divide the set of $\mathcal{T}_i^{\mathrm{A}_{\mathrm{ox}}^{(\mathrm{I})}}$ in two groups. The first group includes the spanning trees that do not contain the edge $\mathrm{B}_{\mathrm{ox}}^{(\mathrm{I})} \to \mathrm{A}_{\mathrm{ox}}^{(\mathrm{I})}$, like the example in Figure S1a. The peculiarity of these spanning trees is that all the corresponding $\mathcal{T}_i^{\mathrm{A}_{\mathrm{ox}}^{(\mathrm{I})}}$ can be expressed in terms of the frequencies $j_{\mathcal{X}}$ of the cycles $\mathcal{X}$ spanning the transition $\mathrm{A}_{\mathrm{ox}}^{(\mathrm{I})} \to \mathrm{B}_{\mathrm{ox}}^{(\mathrm{I})}$. We can therefore leverage the expressions of the cycles' frequencies that we found in the previous Section. For instance, the $\mathcal{T}_i^{\mathrm{A}_{\mathrm{ox}}^{(\mathrm{I})}}$ term corresponding to the spanning tree in Figure S1a can be written as $\mathcal{T}_i^{\mathrm{A}_{\mathrm{ox}}^{(\mathrm{I})}} = \Pi_{\mathcal{B}_3} \times k_{\mathrm{AB,red}} \times k_{\mathrm{BA,ox}}/k_{\mathrm{AB,ox}}$. Gathering all the terms in this first group:

$$\sum_i^{\mathrm{B}_{\mathrm{ox}}^{(\mathrm{I})} \to \mathrm{A}_{\mathrm{ox}}^{(\mathrm{I})} \notin \mathcal{T}_i^{\mathrm{A}_{\mathrm{ox}}^{(\mathrm{I})}}} \mathcal{T}_i^{\mathrm{A}_{\mathrm{ox}}^{(\mathrm{I})}} = \frac{N}{k_{\mathrm{AB,ox}}} \sum_{\mathcal{X}}^{\mathrm{A}_{\mathrm{ox}}^{(\mathrm{I})} \to \mathrm{B}_{\mathrm{ox}}^{(\mathrm{I})} \in \mathcal{X}} j_{\mathcal{X}} = \frac{N}{k_{\mathrm{AB,ox}}} \left(j_{\mathcal{F}_3^\dagger} + j_{\mathcal{F}_4^\dagger} + j_{\mathcal{B}_3} + j_{\mathcal{B}_4} + \sum_i^{\mathrm{A}_{\mathrm{ox}}^{(\mathrm{I})} \to \mathrm{B}_{\mathrm{ox}}^{(\mathrm{I})} \in \mathcal{U}_i^\dagger} j_{\mathcal{U}_i^\dagger} \right), \quad (41)$$

where we used the notation $\sum_i^{\mathrm{B}_{\mathrm{ox}}^{(\mathrm{I})} \to \mathrm{A}_{\mathrm{ox}}^{(\mathrm{I})} \notin \mathcal{T}_i^{\mathrm{A}_{\mathrm{ox}}^{(\mathrm{I})}}}$ to indicate a sum over all the spanning trees rooted in $\mathrm{A}_{\mathrm{ox}}^{(\mathrm{I})}$ that do not include the transition $\mathrm{B}_{\mathrm{ox}}^{(\mathrm{I})} \to \mathrm{A}_{\mathrm{ox}}^{(\mathrm{I})}$, and $\sum_{\mathcal{X}}^{\mathrm{A}_{\mathrm{ox}}^{(\mathrm{I})} \to \mathrm{B}_{\mathrm{ox}}^{(\mathrm{I})} \in \mathcal{X}}$ to indicate a sum over all the cycles that include the transition $\mathrm{A}_{\mathrm{ox}}^{(\mathrm{I})} \to \mathrm{B}_{\mathrm{ox}}^{(\mathrm{I})}$. The last equality leverages that all the possible cycles other than those listed in Figure 2 of the main text are $\mathcal{U}$-cycles, which follows from the fact that sequence S is the only coupling arising in the network of interest.

The second group includes the spanning trees that contain the edge $\mathrm{B}_{\mathrm{ox}}^{(\mathrm{I})} \to \mathrm{A}_{\mathrm{ox}}^{(\mathrm{I})}$, like the example in Figure S1b. The peculiarity of this spanning trees is that all the corresponding $\mathcal{T}_i^{\mathrm{A}_{\mathrm{ox}}^{(\mathrm{I})}}$ can be expressed in terms of the spanning trees $\mathcal{T}_i^{\mathrm{A}_{\mathrm{ox}}^{(\mathrm{I})} - \mathrm{B}_{\mathrm{ox}}^{(\mathrm{I})}}$ of the edge $\mathrm{A}_{\mathrm{ox}}^{(\mathrm{I})} - \mathrm{B}_{\mathrm{ox}}^{(\mathrm{I})}$ (see Figure S1c):

$$\sum_i^{\mathrm{B}_{\mathrm{ox}}^{(\mathrm{I})} \to \mathrm{A}_{\mathrm{ox}}^{(\mathrm{I})} \in \mathcal{T}_i^{\mathrm{A}_{\mathrm{ox}}^{(\mathrm{I})}}} \mathcal{T}_i^{\mathrm{A}_{\mathrm{ox}}^{(\mathrm{I})}} = k_{\mathrm{BA,ox}} \sum_i \mathcal{T}_i^{\mathrm{A}_{\mathrm{ox}}^{(\mathrm{I})} - \mathrm{B}_{\mathrm{ox}}^{(\mathrm{I})}}. \quad (42)$$

By applying Equation (39):

$$[\mathrm{A}_{\mathrm{ox}}^{(\mathrm{I})}]_{\mathrm{ss}} = \frac{1}{N}\left[\frac{N}{k_{\mathrm{AB,ox}}}\left(j_{\mathcal{F}_3^\dagger} + j_{\mathcal{F}_4^\dagger} + j_{\mathcal{B}_3} + j_{\mathcal{B}_4} + \sum_i^{\mathrm{A}_{\mathrm{ox}}^{(\mathrm{I})}\to\mathrm{B}_{\mathrm{ox}}^{(\mathrm{I})}\in\mathcal{U}_i^\dagger} j_{\mathcal{U}_i^\dagger}\right) + k_{\mathrm{BA,ox}}\sum_i \mathcal{T}_i^{\mathrm{A}_{\mathrm{ox}}^{(\mathrm{I})}-\mathrm{B}_{\mathrm{ox}}^{(\mathrm{I})}}\right] \tag{43}$$

S2.3.2 All steady state concentrations

Here, we list the expressions of all $[X]_{\mathrm{ss}}$ computed as described in the previous Section.

$$[\mathrm{A}_{\mathrm{ox}}^{(\mathrm{I})}]_{\mathrm{ss}} = \frac{1}{N}\left[\frac{N}{k_{\mathrm{AB,ox}}}\left(j_{\mathcal{F}_3^\dagger} + j_{\mathcal{F}_4^\dagger} + j_{\mathcal{B}_3} + j_{\mathcal{B}_4} + \sum_i^{\mathrm{A}_{\mathrm{ox}}^{(\mathrm{I})}\to\mathrm{B}_{\mathrm{ox}}^{(\mathrm{I})}\in\mathcal{U}_i^\dagger} j_{\mathcal{U}_i^\dagger}\right) + k_{\mathrm{BA,ox}}\sum_i \mathcal{T}_i^{\mathrm{A}_{\mathrm{ox}}^{(\mathrm{I})}-\mathrm{B}_{\mathrm{ox}}^{(\mathrm{I})}}\right] \tag{44a}$$

$$[\mathrm{B}_{\mathrm{ox}}^{(\mathrm{I})}]_{\mathrm{ss}} = \frac{1}{N}\left[\frac{N}{k_{\mathrm{BA,ox}}}\left(j_{\mathcal{F}_3} + j_{\mathcal{F}_4} + j_{\mathcal{B}_3^\dagger} + j_{\mathcal{B}_4^\dagger} + \sum_i^{\mathrm{B}_{\mathrm{ox}}^{(\mathrm{I})}\to\mathrm{A}_{\mathrm{ox}}^{(\mathrm{I})}\in\mathcal{U}_i} j_{\mathcal{U}_i}\right) + k_{\mathrm{AB,ox}}\sum_i \mathcal{T}_i^{\mathrm{A}_{\mathrm{ox}}^{(\mathrm{I})}-\mathrm{B}_{\mathrm{ox}}^{(\mathrm{I})}}\right] \tag{44b}$$

$$[\mathrm{A}_{\mathrm{ox}}^{(\mathrm{II})}]_{\mathrm{ss}} = \frac{1}{N}\left[\frac{N}{k_{\mathrm{AB,ox}}}\left(j_{\mathcal{F}_1^\dagger} + j_{\mathcal{F}_2^\dagger} + j_{\mathcal{B}_1} + j_{\mathcal{B}_2} + \sum_i^{\mathrm{A}_{\mathrm{ox}}^{(\mathrm{II})}\to\mathrm{B}_{\mathrm{ox}}^{(\mathrm{II})}\in\mathcal{U}_i^\dagger} j_{\mathcal{U}_i^\dagger}\right) + k_{\mathrm{BA,ox}}\sum_i \mathcal{T}_i^{\mathrm{A}_{\mathrm{ox}}^{(\mathrm{II})}-\mathrm{B}_{\mathrm{ox}}^{(\mathrm{II})}}\right] \tag{44c}$$

$$[\mathrm{B}_{\mathrm{ox}}^{(\mathrm{II})}]_{\mathrm{ss}} = \frac{1}{N}\left[\frac{N}{k_{\mathrm{BA,ox}}}\left(j_{\mathcal{F}_1} + j_{\mathcal{F}_2} + j_{\mathcal{B}_1^\dagger} + j_{\mathcal{B}_2^\dagger} + \sum_i^{\mathrm{B}_{\mathrm{ox}}^{(\mathrm{II})}\to\mathrm{A}_{\mathrm{ox}}^{(\mathrm{II})}\in\mathcal{U}_i} j_{\mathcal{U}_i}\right) + k_{\mathrm{AB,ox}}\sum_i \mathcal{T}_i^{\mathrm{A}_{\mathrm{ox}}^{(\mathrm{II})}-\mathrm{B}_{\mathrm{ox}}^{(\mathrm{II})}}\right] \tag{44d}$$

$$[\mathrm{A}_{\mathrm{red}}^{(\mathrm{I})}]_{\mathrm{ss}} = \frac{1}{N}\left[\frac{N}{k_{\mathrm{AB,red}}}\left(j_{\mathcal{F}_1} + j_{\mathcal{F}_4} + j_{\mathcal{B}_1^\dagger} + j_{\mathcal{B}_4^\dagger} + \sum_i^{\mathrm{A}_{\mathrm{red}}^{(\mathrm{I})}\to\mathrm{B}_{\mathrm{red}}^{(\mathrm{I})}\in\mathcal{U}_i} j_{\mathcal{U}_i}\right) + k_{\mathrm{BA,red}}\sum_i \mathcal{T}_i^{\mathrm{A}_{\mathrm{red}}^{(\mathrm{I})}-\mathrm{B}_{\mathrm{red}}^{(\mathrm{I})}}\right] \tag{44e}$$

$$[\mathrm{B}_{\mathrm{red}}^{(\mathrm{I})}]_{\mathrm{ss}} = \frac{1}{N}\left[\frac{N}{k_{\mathrm{BA,red}}}\left(j_{\mathcal{F}_1^\dagger} + j_{\mathcal{F}_4^\dagger} + j_{\mathcal{B}_1} + j_{\mathcal{B}_4} + \sum_i^{\mathrm{B}_{\mathrm{red}}^{(\mathrm{I})}\to\mathrm{A}_{\mathrm{red}}^{(\mathrm{I})}\in\mathcal{U}_i^\dagger} j_{\mathcal{U}_i^\dagger}\right) + k_{\mathrm{AB,red}}\sum_i \mathcal{T}_i^{\mathrm{A}_{\mathrm{red}}^{(\mathrm{I})}-\mathrm{B}_{\mathrm{red}}^{(\mathrm{I})}}\right] \tag{44f}$$

$$[\mathrm{A}^{(\mathrm{II})}_{\mathrm{red}}]_{\mathrm{ss}} = \frac{1}{N}\left[\frac{N}{k_{\mathrm{AB,red}}}\left(j_{\mathcal{F}_2} + j_{\mathcal{F}_3} + j_{\mathcal{B}_2^\dagger} + j_{\mathcal{B}_3^\dagger} + \sum_i^{\mathrm{A}^{(\mathrm{II})}_{\mathrm{red}}\to\mathrm{B}^{(\mathrm{II})}_{\mathrm{red}}\in\mathcal{U}_i} j_{\mathcal{U}_i}\right) + k_{\mathrm{BA,red}}\sum_i \mathcal{T}_i^{\mathrm{A}^{(\mathrm{II})}_{\mathrm{red}}-\mathrm{B}^{(\mathrm{II})}_{\mathrm{red}}}\right] \tag{44g}$$

$$[\mathrm{B}^{(\mathrm{II})}_{\mathrm{red}}]_{\mathrm{ss}} = \frac{1}{N}\left[\frac{N}{k_{\mathrm{BA,red}}}\left(j_{\mathcal{F}_2^\dagger} + j_{\mathcal{F}_3^\dagger} + j_{\mathcal{B}_2} + j_{\mathcal{B}_3} + \sum_i^{\mathrm{B}^{(\mathrm{II})}_{\mathrm{red}}\to\mathrm{A}^{(\mathrm{II})}_{\mathrm{red}}\in\mathcal{U}_i^\dagger} j_{\mathcal{U}_i^\dagger}\right) + k_{\mathrm{AB,red}}\sum_i \mathcal{T}_i^{\mathrm{A}^{(\mathrm{II})}_{\mathrm{red}}-\mathrm{B}^{(\mathrm{II})}_{\mathrm{red}}}\right] \tag{44h}$$

S2.3.3 Computation of $\frac{[\mathrm{A}^{(\mathrm{I})}_{\mathrm{ox}}]_{\mathrm{ss}}+[\mathrm{A}^{(\mathrm{II})}_{\mathrm{ox}}]_{\mathrm{ss}}}{[\mathrm{B}^{(\mathrm{I})}_{\mathrm{ox}}]_{\mathrm{ss}}+[\mathrm{B}^{(\mathrm{II})}_{\mathrm{ox}}]_{\mathrm{ss}}}$ and $\frac{[\mathrm{A}^{(\mathrm{I})}_{\mathrm{red}}]_{\mathrm{ss}}+[\mathrm{A}^{(\mathrm{II})}_{\mathrm{red}}]_{\mathrm{ss}}}{[\mathrm{B}^{(\mathrm{I})}_{\mathrm{red}}]_{\mathrm{ss}}+[\mathrm{B}^{(\mathrm{II})}_{\mathrm{red}}]_{\mathrm{ss}}}$

We are now in the position to compute the ratios in Equation (37) using the expressions in Equation (44). To keep the notation concise, in the following we will use $\sum_i j_{\mathcal{F}_i} = j_{\mathcal{F}_1} + j_{\mathcal{F}_2} + j_{\mathcal{F}_3} + j_{\mathcal{F}_4}$, $\sum_i j_{\mathcal{B}_i} = j_{\mathcal{B}_1} + j_{\mathcal{B}_2} + j_{\mathcal{B}_3} + j_{\mathcal{B}_4}$, and $\sum_i^{\mathrm{B_{ox}}\to\mathrm{A_{ox}}} j_{\mathcal{U}_i} = \sum_i^{\mathrm{B}^{(\mathrm{I})}_{\mathrm{ox}}\to\mathrm{A}^{(\mathrm{I})}_{\mathrm{ox}}\in\mathcal{U}_i} j_{\mathcal{U}_i} + \sum_i^{\mathrm{B}^{(\mathrm{II})}_{\mathrm{ox}}\to\mathrm{A}^{(\mathrm{II})}_{\mathrm{ox}}\in\mathcal{U}_i} j_{\mathcal{U}_i}$.

$$\frac{[\mathrm{A}^{(\mathrm{I})}_{\mathrm{ox}}]_{\mathrm{ss}}+[\mathrm{A}^{(\mathrm{II})}_{\mathrm{ox}}]_{\mathrm{ss}}}{[\mathrm{B}^{(\mathrm{I})}_{\mathrm{ox}}]_{\mathrm{ss}}+[\mathrm{B}^{(\mathrm{II})}_{\mathrm{ox}}]_{\mathrm{ss}}} = \frac{k_{\mathrm{BA,ox}}}{k_{\mathrm{AB,ox}}} \times \frac{\sum_i j_{\mathcal{F}_i^\dagger} + \sum_i j_{\mathcal{B}_i} + \sum_i^{\mathrm{A_{ox}}\to\mathrm{B_{ox}}} j_{\mathcal{U}_i^\dagger} + \frac{k_{\mathrm{BA,ox}}k_{\mathrm{AB,ox}}}{N}\sum_i(\mathcal{T}_i^{\mathrm{A}^{(\mathrm{I})}_{\mathrm{ox}}-\mathrm{B}^{(\mathrm{I})}_{\mathrm{ox}}} + \mathcal{T}_i^{\mathrm{A}^{(\mathrm{II})}_{\mathrm{ox}}-\mathrm{B}^{(\mathrm{II})}_{\mathrm{ox}}})}{\sum_i j_{\mathcal{F}_i} + \sum_i j_{\mathcal{B}_i^\dagger} + \sum_i^{\mathrm{B_{ox}}\to\mathrm{A_{ox}}} j_{\mathcal{U}_i} + \frac{k_{\mathrm{BA,ox}}k_{\mathrm{AB,ox}}}{N}\sum_i(\mathcal{T}_i^{\mathrm{A}^{(\mathrm{I})}_{\mathrm{ox}}-\mathrm{B}^{(\mathrm{I})}_{\mathrm{ox}}} + \mathcal{T}_i^{\mathrm{A}^{(\mathrm{II})}_{\mathrm{ox}}-\mathrm{B}^{(\mathrm{II})}_{\mathrm{ox}}})} = \tag{45a}$$

$$= \frac{k_{\mathrm{BA,ox}}}{k_{\mathrm{AB,ox}}} \times \frac{e^{-2\Omega_{\mathrm{BV}}\Delta E}\sum_i j_{\mathcal{F}_i} + \sum_i j_{\mathcal{B}_i} + \sum_i^{\mathrm{B_{ox}}\to\mathrm{A_{ox}}} j_{\mathcal{U}_i} + \frac{k_{\mathrm{BA,ox}}k_{\mathrm{AB,ox}}}{N}\sum_i(\mathcal{T}_i^{\mathrm{A}^{(\mathrm{I})}_{\mathrm{ox}}-\mathrm{B}^{(\mathrm{I})}_{\mathrm{ox}}} + \mathcal{T}_i^{\mathrm{A}^{(\mathrm{II})}_{\mathrm{ox}}-\mathrm{B}^{(\mathrm{II})}_{\mathrm{ox}}})}{\sum_i j_{\mathcal{F}_i} + e^{-2\Omega_{\mathrm{BV}}\Delta E}\sum_i j_{\mathcal{B}_i} + \sum_i^{\mathrm{B_{ox}}\to\mathrm{A_{ox}}} j_{\mathcal{U}_i} + \frac{k_{\mathrm{BA,ox}}k_{\mathrm{AB,ox}}}{N}\sum_i(\mathcal{T}_i^{\mathrm{A}^{(\mathrm{I})}_{\mathrm{ox}}-\mathrm{B}^{(\mathrm{I})}_{\mathrm{ox}}} + \mathcal{T}_i^{\mathrm{A}^{(\mathrm{II})}_{\mathrm{ox}}-\mathrm{B}^{(\mathrm{II})}_{\mathrm{ox}}})} =$$
$$= K_{\mathrm{ox}} \times \left\{\frac{qe^{-2\Omega_{\mathrm{BV}}\Delta E} + 1 + \Psi_{\mathrm{ox}}}{q + e^{-2\Omega_{\mathrm{BV}}\Delta E} + \Psi_{\mathrm{ox}}}\right\},$$

$$\frac{[\mathrm{A}^{(\mathrm{I})}_{\mathrm{red}}]_{\mathrm{ss}}+[\mathrm{A}^{(\mathrm{II})}_{\mathrm{red}}]_{\mathrm{ss}}}{[\mathrm{B}^{(\mathrm{I})}_{\mathrm{red}}]_{\mathrm{ss}}+[\mathrm{B}^{(\mathrm{II})}_{\mathrm{red}}]_{\mathrm{ss}}} = \frac{k_{\mathrm{BA,red}}}{k_{\mathrm{AB,red}}} \times \frac{\sum_i j_{\mathcal{F}_i} + \sum_i j_{\mathcal{B}_i^\dagger} + \sum_i^{\mathrm{A_{red}}\to\mathrm{B_{red}}} j_{\mathcal{U}_i} + \frac{k_{\mathrm{BA,red}}k_{\mathrm{AB,red}}}{N}\sum_i(\mathcal{T}_i^{\mathrm{A}^{(\mathrm{I})}_{\mathrm{red}}-\mathrm{B}^{(\mathrm{I})}_{\mathrm{red}}} + \mathcal{T}_i^{\mathrm{A}^{(\mathrm{II})}_{\mathrm{red}}-\mathrm{B}^{(\mathrm{II})}_{\mathrm{red}}})}{\sum_i j_{\mathcal{F}_i^\dagger} + \sum_i j_{\mathcal{B}_i} + \sum_i^{\mathrm{B_{red}}\to\mathrm{A_{red}}} j_{\mathcal{U}_i^\dagger} + \frac{k_{\mathrm{BA,red}}k_{\mathrm{AB,red}}}{N}\sum_i(\mathcal{T}_i^{\mathrm{A}^{(\mathrm{I})}_{\mathrm{red}}-\mathrm{B}^{(\mathrm{I})}_{\mathrm{red}}} + \mathcal{T}_i^{\mathrm{A}^{(\mathrm{II})}_{\mathrm{red}}-\mathrm{B}^{(\mathrm{II})}_{\mathrm{red}}})} = \tag{45b}$$

$$= \frac{k_{\mathrm{BA,red}}}{k_{\mathrm{AB,red}}} \times \frac{\sum_i j_{\mathcal{F}_i} + e^{-2\Omega_{\mathrm{BV}}\Delta E}\sum_i j_{\mathcal{B}_i} + \sum_i^{\mathrm{A_{red}}\to\mathrm{B_{red}}} j_{\mathcal{U}_i} + \frac{k_{\mathrm{BA,red}}k_{\mathrm{AB,red}}}{N}\sum_i(\mathcal{T}_i^{\mathrm{A}^{(\mathrm{I})}_{\mathrm{red}}-\mathrm{B}^{(\mathrm{I})}_{\mathrm{red}}} + \mathcal{T}_i^{\mathrm{A}^{(\mathrm{II})}_{\mathrm{red}}-\mathrm{B}^{(\mathrm{II})}_{\mathrm{red}}})}{e^{-2\Omega_{\mathrm{BV}}\Delta E}\sum_i j_{\mathcal{F}_i} + \sum_i^{\mathrm{A_{red}}\to\mathrm{B_{red}}} j_{\mathcal{B}_i} + \sum_i^{\mathrm{A_{red}}\to\mathrm{B_{red}}} j_{\mathcal{U}_i} + \frac{k_{\mathrm{BA,red}}k_{\mathrm{AB,red}}}{N}\sum_i(\mathcal{T}_i^{\mathrm{A}^{(\mathrm{I})}_{\mathrm{red}}-\mathrm{B}^{(\mathrm{I})}_{\mathrm{red}}} + \mathcal{T}_i^{\mathrm{A}^{(\mathrm{II})}_{\mathrm{red}}-\mathrm{B}^{(\mathrm{II})}_{\mathrm{red}}})} =$$
$$= K_{\mathrm{red}} \times \left\{\frac{q + e^{-2\Omega_{\mathrm{BV}}\Delta E} + \Psi_{\mathrm{red}}}{qe^{-2\Omega_{\mathrm{BV}}\Delta E} + 1 + \Psi_{\mathrm{red}}}\right\},$$

where

$$\Psi_{\mathrm{ox}} = \frac{\sum_i^{\mathrm{B_{ox}}\to\mathrm{A_{ox}}} j_{\mathcal{U}_i}}{\sum_i j_{\mathcal{B}_i}} + \frac{k_{\mathrm{BA,ox}} k_{\mathrm{AB,ox}}}{N \sum_i j_{\mathcal{B}_i}} \sum_i (\mathcal{T}_i^{\mathrm{A_{ox}^{(I)}}-\mathrm{B_{ox}^{(I)}}} + \mathcal{T}_i^{\mathrm{A_{ox}^{(II)}}-\mathrm{B_{ox}^{(II)}}}) \tag{46a}$$

$$\Psi_{\mathrm{red}} = \frac{\sum_i^{\mathrm{A_{red}}\to\mathrm{B_{red}}} j_{\mathcal{U}_i}}{\sum_i j_{\mathcal{B}_i}} + \frac{k_{\mathrm{BA,red}} k_{\mathrm{AB,red}}}{N \sum_i j_{\mathcal{B}_i}} \sum_i (\mathcal{T}_i^{\mathrm{A_{red}^{(I)}}-\mathrm{B_{red}^{(I)}}} + \mathcal{T}_i^{\mathrm{A_{red}^{(II)}}-\mathrm{B_{red}^{(II)}}}) \tag{46b}$$

and we recognized q as defined in Equation (15). We relied on cycle's properties discussed in Section S2.1 to simplify the above expressions.

S3 Numerical investigation

The network was modeled according to the following mass action kinetics, describing the rate at which the concentration of each species in the network in Figure 1b in the main text varies in time:

$$\frac{d[\mathrm{A}_{\mathrm{ox}}^{(\mathrm{I})}]}{dt} = k_{\mathrm{BA,ox}} \cdot [\mathrm{B}_{\mathrm{ox}}^{(\mathrm{I})}] - k_{\mathrm{AB,ox}} \cdot [\mathrm{A}_{\mathrm{ox}}^{(\mathrm{I})}] + k_{-1} \cdot [\mathrm{A}_{\mathrm{red}}^{(\mathrm{I})}] - k_{+1} \cdot [\mathrm{A}_{\mathrm{ox}}^{(\mathrm{I})}] + k_{dA} \cdot [\mathrm{A}_{\mathrm{ox}}^{(\mathrm{II})}] - k_{dA} \cdot [\mathrm{A}_{\mathrm{ox}}^{(\mathrm{I})}] \tag{47}$$

$$\frac{d[\mathrm{A}_{\mathrm{ox}}^{(\mathrm{II})}]}{dt} = k_{\mathrm{BA,ox}} \cdot [\mathrm{B}_{\mathrm{ox}}^{(\mathrm{II})}] - k_{\mathrm{AB,ox}} \cdot [\mathrm{A}_{\mathrm{ox}}^{(\mathrm{II})}] + k_{-3} \cdot [\mathrm{A}_{\mathrm{red}}^{(\mathrm{I})}] - k_{+3} \cdot [\mathrm{A}_{\mathrm{ox}}^{(\mathrm{II})}] + k_{dA} \cdot [\mathrm{A}_{\mathrm{ox}}^{(\mathrm{I})}] - k_{dA} \cdot [\mathrm{A}_{\mathrm{ox}}^{(\mathrm{II})}] \tag{48}$$

$$\frac{d[\mathrm{B}_{\mathrm{ox}}^{(\mathrm{I})}]}{dt} = -k_{\mathrm{BA,ox}} \cdot [\mathrm{B}_{\mathrm{ox}}^{(\mathrm{I})}] + k_{\mathrm{AB,ox}} \cdot [\mathrm{A}_{\mathrm{ox}}^{(\mathrm{I})}] + k_{-2} \cdot [\mathrm{B}_{\mathrm{red}}^{(\mathrm{I})}] - k_{+2} \cdot [\mathrm{B}_{\mathrm{ox}}^{(\mathrm{I})}] + k_{dB} \cdot [\mathrm{B}_{\mathrm{ox}}^{(\mathrm{II})}] - k_{dB} \cdot [\mathrm{B}_{\mathrm{ox}}^{(\mathrm{I})}] \tag{49}$$

$$\frac{d[\mathrm{B}_{\mathrm{ox}}^{(\mathrm{II})}]}{dt} = -k_{\mathrm{BA,ox}} \cdot [\mathrm{B}_{\mathrm{ox}}^{(\mathrm{II})}] + k_{\mathrm{AB,ox}} \cdot [\mathrm{A}_{\mathrm{ox}}^{(\mathrm{II})}] + k_{-4} \cdot [\mathrm{B}_{\mathrm{red}}^{(\mathrm{II})}] - k_{+4} \cdot [\mathrm{B}_{\mathrm{red}}^{(\mathrm{II})}] + k_{dB} \cdot [\mathrm{B}_{\mathrm{ox}}^{(\mathrm{I})}] - k_{dB} \cdot [\mathrm{B}_{\mathrm{ox}}^{(\mathrm{II})}] \tag{50}$$

$$\frac{d[\mathrm{A}_{\mathrm{red}}^{(\mathrm{I})}]}{dt} = k_{\mathrm{AB,red}} \cdot [\mathrm{A}_{\mathrm{red}}^{(\mathrm{I})}] + k_{\mathrm{BA,red}} \cdot [\mathrm{B}_{\mathrm{red}}^{(\mathrm{I})}] - k_{-1} \cdot [\mathrm{A}_{\mathrm{red}}^{(\mathrm{I})}] + k_{+1} \cdot [\mathrm{A}_{\mathrm{ox}}^{(\mathrm{I})}] + k_{dA} \cdot [\mathrm{A}_{\mathrm{red}}^{(\mathrm{II})}] - k_{dA} \cdot [\mathrm{A}_{\mathrm{red}}^{(\mathrm{I})}] \tag{51}$$

$$\frac{d[\mathrm{A}_{\mathrm{red}}^{(\mathrm{II})}]}{dt} = -k_{\mathrm{AB,red}} \cdot [\mathrm{A}_{\mathrm{red}}^{(\mathrm{II})}] + k_{\mathrm{BA,red}} \cdot [\mathrm{B}_{\mathrm{red}}^{(\mathrm{II})}] - k_{-3} \cdot [\mathrm{A}_{\mathrm{red}}^{(\mathrm{II})}] + k_{+3} \cdot [\mathrm{A}_{\mathrm{ox}}^{(\mathrm{II})}] - k_{dA} \cdot [\mathrm{A}_{\mathrm{red}}^{(\mathrm{II})}] + k_{dA} \cdot [\mathrm{A}_{\mathrm{red}}^{(\mathrm{I})}] \tag{52}$$

$$\frac{d[\mathrm{B}_{\mathrm{red}}^{(\mathrm{I})}]}{dt} = k_{\mathrm{AB,red}} \cdot [\mathrm{A}_{\mathrm{red}}^{(\mathrm{I})}] - k_{\mathrm{BA,red}} \cdot [\mathrm{B}_{\mathrm{red}}^{(\mathrm{I})}] - k_{-2} \cdot [\mathrm{B}_{\mathrm{red}}^{(\mathrm{I})}] + k_{+2} \cdot [\mathrm{B}_{\mathrm{ox}}^{(\mathrm{I})}] + k_{dB} \cdot [\mathrm{B}_{\mathrm{red}}^{(\mathrm{II})}] - k_{dB} \cdot [\mathrm{B}_{\mathrm{red}}^{(\mathrm{I})}] \tag{53}$$

$$\frac{d[\mathrm{B}_{\mathrm{red}}^{(\mathrm{II})}]}{dt} = k_{\mathrm{AB,red}} \cdot [\mathrm{A}_{\mathrm{red}}^{(\mathrm{II})}] - k_{\mathrm{BA,red}} \cdot [\mathrm{B}_{\mathrm{red}}^{(\mathrm{II})}] - k_{-4} \cdot [\mathrm{B}_{\mathrm{red}}^{(\mathrm{II})}] + k_{+4} \cdot [\mathrm{B}_{\mathrm{ox}}^{(\mathrm{II})}] - k_{dB} \cdot [\mathrm{B}_{\mathrm{red}}^{(\mathrm{II})}] + k_{dB} \cdot [\mathrm{B}_{\mathrm{red}}^{(\mathrm{I})}] \tag{54}$$

where k_i is the rate constant of reaction i, and the apex I or II refers to the two compartments. In all simulations performed, we started with an initial concentration of 0.25 M for all species so that the total concentration is fixed at 2 M. The diffusion constants of all species are set to be the same ($k_{dA} = k_{dB} = k_d$), when not otherwise stated. The rates associated with reactions 1-4 were calculated according to equations (3). All simulations were performed considering T = 298 K, R = 8.314 J K^{-1} mol^{-1} F = 9.6485 $\cdot$ 10^4 C mol^{-1} and $\alpha = 0.5$. The simulated time is expressed in seconds (s) and the concentration in mol L^{-1}.

A python code was implemented to solve the above ordinary differential equations (ODEs), which were solved numerically using the solve-ivp function and using 'LSODA' as method, from the scipy.integrate module. [1]

[1] See also: https://docs.scipy.org/doc/scipy/reference/generated/scipy.integrate.LSODA.html

To investigate network directionality, we monitored the fluxes of chemical reactions, expressed as:

$$\Phi_5 = k_{\mathrm{BA,red}} \cdot [\mathrm{B}^{(\mathrm{I})}_{\mathrm{red}}] - k_{\mathrm{AB,red}} \cdot [\mathrm{A}^{(\mathrm{I})}_{\mathrm{red}}] \tag{55}$$

$$\Phi_6 = k_{\mathrm{BA,ox}} \cdot [\mathrm{B}^{(\mathrm{I})}_{\mathrm{ox}}] - k_{\mathrm{AB,ox}} \cdot [\mathrm{A}^{(\mathrm{I})}_{\mathrm{ox}}] \tag{56}$$

$$\Phi_7 = k_{\mathrm{BA,red}} \cdot [\mathrm{B}^{(\mathrm{II})}_{\mathrm{red}}] - k_{\mathrm{AB,red}} \cdot [\mathrm{A}^{(\mathrm{II})}_{\mathrm{red}}] \tag{57}$$

$$\Phi_8 = k_{\mathrm{BA,ox}} \cdot [\mathrm{B}^{(\mathrm{II})}_{\mathrm{ox}}] - k_{\mathrm{AB,ox}} \cdot [\mathrm{A}^{(\mathrm{II})}_{\mathrm{ox}}] \tag{58}$$

To produce the data reported in the main text and SI, the parameter under investigation was varied, while others remained constant or changed according to microscopic reversibility constraints if needed. ODEs were solved for each specific value of the parameters. To ensure that a steady state was reached, a sufficiently extended duration window was selected for the simulation. Species concentration were plotted over time to confirm the attainment of a steady state. The final flux values corresponding to steady-state concentrations was picked automatically and plotted as a function of the variable parameter under investigation.

The thermodynamic consistency of the model was monitored, by verifying the following microscopic reversibility constraints, indicating that within a closed cycle that does not involve a net transport of electrons from one electrode to the other, the product of all the equilibrium constants equals 1:

$$\frac{k_1 \cdot k_{\mathrm{AB,red}} \cdot k_{-2} \cdot k_{\mathrm{BA,ox}}}{k_{-1} \cdot k_{\mathrm{BA,red}} \cdot k_{+2} \cdot k_{\mathrm{AB,ox}}} = 1 \tag{59}$$

$$\frac{k_{+4} \cdot k_{\mathrm{AB,red}} \cdot k_{-3} \cdot k_{\mathrm{BA,ox}}}{k_{-4} \cdot k_{\mathrm{BA,red}} \cdot k_{+3} \cdot k_{\mathrm{AB,ox}}} = 1 \tag{60}$$

The parameters reported in Table S1 were used to produce Figures 4a-c in the main text and Figure S2. While in in the main text we reported the sum of fluxes (Φ_6+Φ_8 and Φ_5+Φ_7), here we report the individual fluxes to offer greater insights.

Table S1: Parameters used to produce Figure 4a-c and Figure S2.

Parameter	Fluxes vs E_{II}	Fluxes vs k_{d}	Fluxes vs $K_{\mathrm{ox}}/K_{\mathrm{red}}$
E_{I}	-0.2	-0.4	-0.4
E_{II}	variable	0.4	0.4
E°_{A}	-0.2	-0.2	-0.2
E°_{B}	0.0365[a]	0.0365[a]	variable[a]
$k_{\mathrm{AB,ox}}$	1	1	1
$k_{\mathrm{AB,red}}$	100	100	1
$k_{\mathrm{BA,ox}}$	100	100	variable[b]
$k_{\mathrm{BA,red}}$	1	1	1
k_{d}	0.1	variable	0.1
k_{e}	10^5	10^5	10^5

[a] Fixed according to to the microscopic reversibility constraint defined by 9. [b] K_{ox} was varied by changing $k_{\mathrm{BA,ox}}$ while keeping $k_{\mathrm{AB,ox}}$ constant.

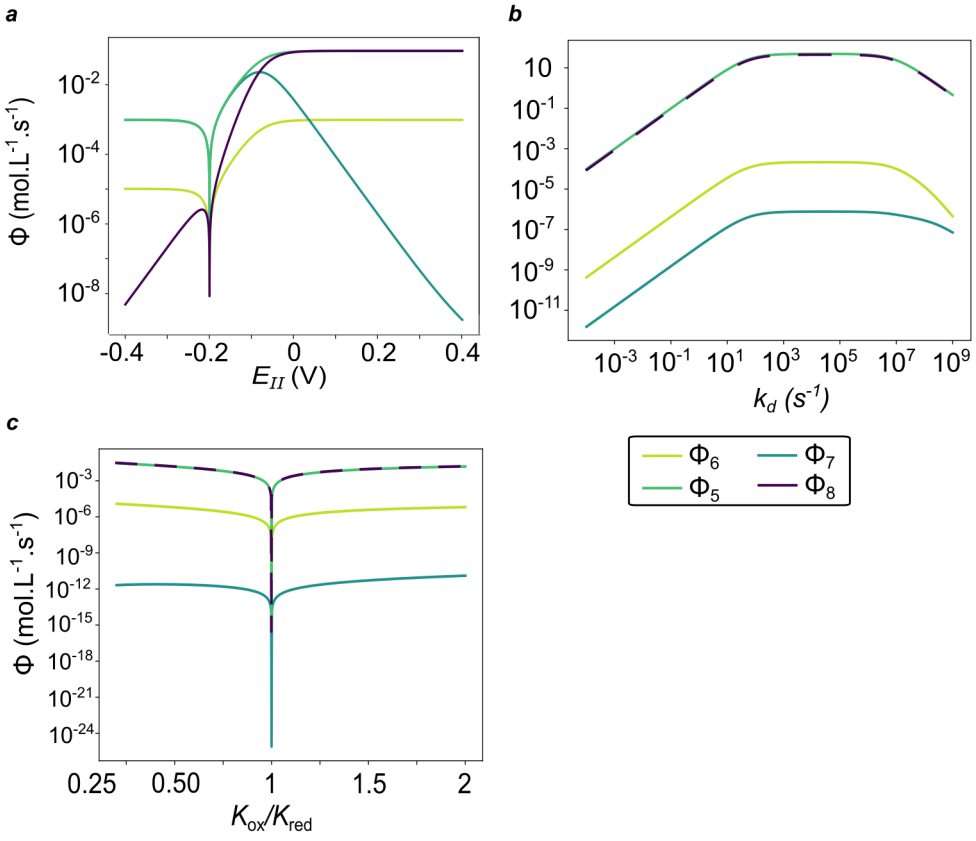

Figure S2: Reaction fluxes on a logarithmic scale. Logarithm of the absolute value of reaction fluxes upon varying (***a***) the electrode potential, E_{II}; (***b***) the diffusion constant k_d (logarithmic scale); (***c***) the ratio of equilibrium constants $K_{\mathrm{ox}}/K_{\mathrm{red}}$.

The parameters reported in Table S2 were used to produce Figure 4c and Figure S3. We showcase the flux variations as a function of the diffusion constant within a symmetrical regime (where k_{dA}=k_{dB}=k_d), and observe how the onset-offset of bell-shaped flux curves reported in Figure 4c - coinciding with Case 1 - changes upon varying the rate of electrochemical reactions (Case 2) and chemical reactions.

Table S2: Parameters used to produce Figure 4c and S3

Parameter	Case 1 (full line)	Case 2 (dashed line)	Case 3 (dotted line)
E_{I}	-0.4	-0.4	-0.4
E_{II}	0.4	0.4	0.4
E°_{A}	-0.2	-0.2	-0.2
E°_{B}	0.0365[a]	0.0365[a]	0.0365[a]
$k_{\mathrm{AB,ox}}$	1	1	0.1
$k_{\mathrm{AB,red}}$	100	100	10
$k_{\mathrm{BA,ox}}$	100	100	10
$k_{\mathrm{BA,red}}$	1	1	0.1
k_{d}	variable	variable	variable
k_{e}	10^5	10^6	10^5

[a] Fixed according to to the microscopic reversibility constraint defined by equation 9.

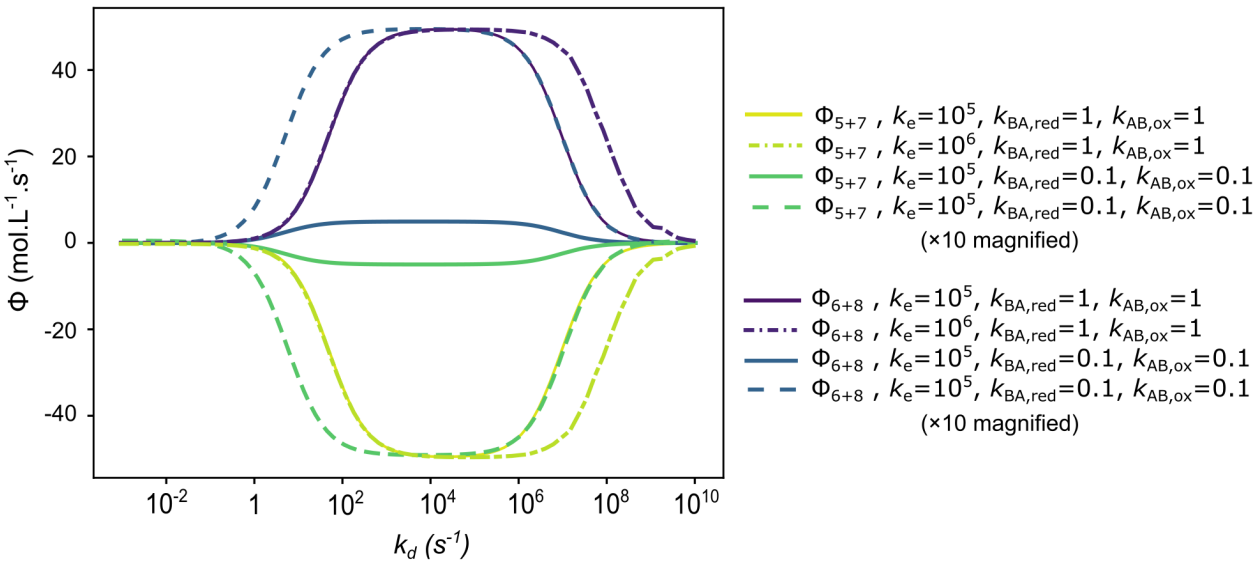

Figure S3: Steady-state fluxes Φ_6+Φ_8 and Φ_5+Φ_7 obtained upon varying k_{d}. Case 1 (full line) coincides with the curve shown in the main text (Figure 4c); in Case 2 (dash-dot lines) the electrochemical processes are one-order-of-magnitude faster with respect to Case 1; in Case 3 (blue and green lines) chemical reactions are one-order-of-magnitude slower than Case 1. To facilitate the comparison with other cases, case 3 was also plotted with a 10-times magnification (blue and green dotted lines).

The parameters in Table S3 were used to produce the data shown in Figure S4. In simulations a-c we show how the fluxes as a function of the diffusion constant are affected by different electrode potential differences, ΔE; moreover, simulations d-g report on cases where rate constants of chemical steps or diffusion were changed, to install - eventually - information ratchet effects.

Table S3: Parameters used to produce Figure 4c,d and S4.

Parameter	a	b	c	d	e	f	g
E_{I}	-0.4	-0.4	-0.4	-0.4	-0.4	-0.4	-0.4
E_{II}	0.4	-0.2	-0.3	0.2	0.2	0.2	0.2
E°_{A}	-0.2	-0.2	-0.2	-0.2	-0.2	-0.2	-0.2
E°_{B}	0.0365[a]	0.0365[a]	0.0365[a]	variable[a]	variable[a]	variable[a]	variable[a]
$k_{\mathrm{AB,ox}}$	1	1	1	1	1000	1000	1000
$k_{\mathrm{AB,red}}$	100	100	100	1000	1	1	1
$k_{\mathrm{BA,ox}}$	100	100	100	variable[a]	variable[b]	variable[b]	variable[b]
$k_{\mathrm{BA,red}}$	1	1	1	1000	1	1	1
k_{d}	variable	variable	variable	0.1	0.1	asymmetric[c]	asymmetric[c]
k_{e}	10^5	10^5	10^5	10^5	10^5	10^5	10^5

[a] E°_{B} was calculated according to the constraint defined by equation 9. [b] K_{ox} was varied intentionally, and the forward rate constant of oxidized species was fixed ($k_{\mathrm{AB,ox}}$), thus $k_{\mathrm{BA,ox}}$ varies according to the equilibrium constant relation. [c] Asymmetrical diffusion was enabled here so that species A diffused differently than species B. For panel ***f***, k_{dA}=100, k_{dB}=0.1 and for panel ***g***, k_{dA}=0.1 and k_{dB}=100.

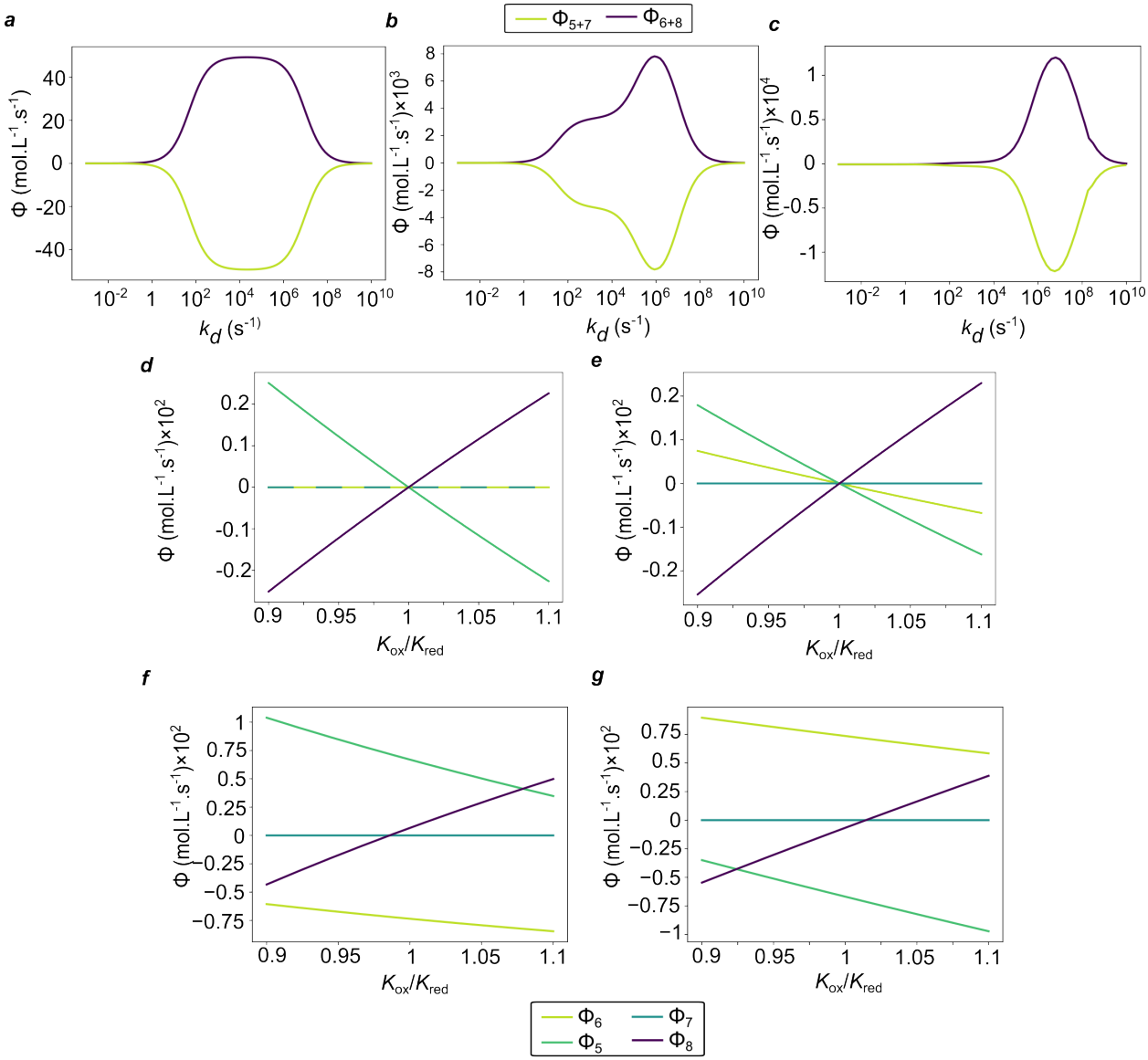

Figure S4: Additional results on reaction fluxes. Panels ***a-c***. Changes in the total fluxes of reactions 5+7 and 6+8 as a function of k_d at different electrochemical gradients ΔE, being 0.8, 0.2, and 0.1, respectively. Panels ***d-g*** Changes in the individual fluxes of reactions 5, 6, 7, and 8 under different conditions. Panels ***d*** and ***e*** show the K_{ox}/K_{red}-dependence upon inverting the rate of reactions 5 and 7 with respect to 6 and 8, the former being faster in panel ***d***, and slower in panel ***e***. In panels ***f*** and ***g*** is show the K_{ox}/K_{red}-dependence upon inverting the diffusion rates for species A and B; in panel ***f***, A was set to diffuse 1000 times faster than B. In panel ***g***, B was set to diffuse 1000 times faster than A. In both panel ***f*** and ***g*** reaction 6 and 8 were chosen to be faster than 5 and 7.

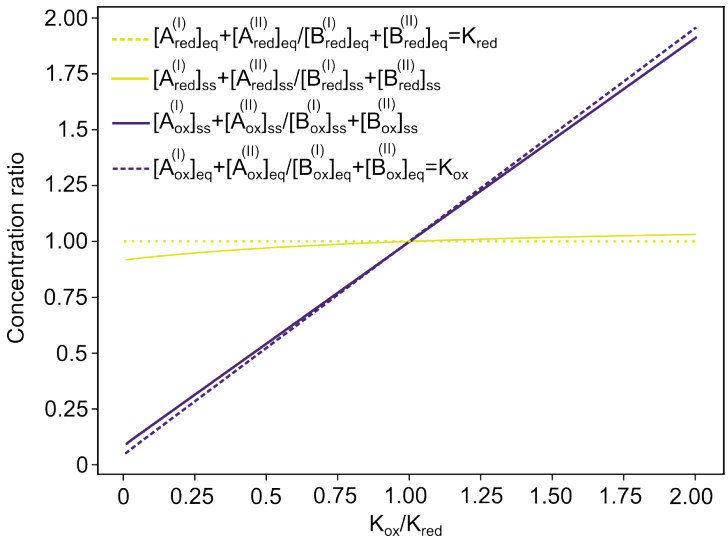

Figure S5: Testing the nonequilibrium pumping equality. Variations of steady-state concentration ratio of A to B in both oxidized and reduced states, are plotted relative to the equilibrium constant ratio K_{ox}/K_{red}. Additionally, graphs of $\frac{[\mathrm{A}^{(\mathrm{I})}_{\mathrm{ox}}]_{\mathrm{eq}}+[\mathrm{A}^{(\mathrm{II})}_{\mathrm{ox}}]_{\mathrm{eq}}}{[\mathrm{B}^{(\mathrm{I})}_{\mathrm{ox}}]_{\mathrm{eq}}+[\mathrm{B}^{(\mathrm{II})}_{\mathrm{ox}}]_{\mathrm{eq}}} = K_{\mathrm{ox}}$ and $\frac{[\mathrm{A}^{(\mathrm{I})}_{\mathrm{red}}]_{\mathrm{eq}}+[\mathrm{A}^{(\mathrm{II})}_{\mathrm{red}}]_{\mathrm{eq}}}{[\mathrm{B}^{(\mathrm{I})}_{\mathrm{red}}]_{\mathrm{eq}}+[\mathrm{B}^{(\mathrm{II})}_{\mathrm{red}}]_{\mathrm{eq}}} = K_{\mathrm{red}}$ are included to examine deviations from the equilibrium case.

References

(S1) Sangchai, T.; Al Shehimy, S.; Penocchio, E.; Ragazzon, G. (2023). Artificial Molecular Ratchets: Tools Enabling Endergonic Processes. Angew. Chem. Int. Ed. 62, e202309501. 10.1002/anie.202309501.

(S2) Bard, A. J.; Faulkner, L. R. (2001). Electrochemical Methods (John Wiley & Sons).

(S3) Ragazzon, G.; Malferrari, M.; Arduini, A.; Secchi, A.; Rapino, S.; Silvi, S.; Credi, A. (2023). Autonomous Non-Equilibrium Self-Assembly and Molecular Movements Powered by Electrical Energy. Angew. Chem. Int. Ed. 62, e202214265. 10.1002/anie.202214265.

(S4) Cook, S. K.; Horrocks, B. R. (2017). Heterogeneous Electron-Transfer Rates for the Reduction of Viologen Derivatives at Platinum and Bismuth Electrodes in Acetonitrile. ChemElectroChem 4, 320–331. 10.1002/celc.201600536.

(S5) Astumian, R. D. (2010). Thermodynamics and Kinetics of Molecular Motors. Biophys. J. 98, 2401–2409. 10.1016/j.bpj.2010.02.040.

(S6) Van den Broeck, C.; Esposito, M. (2015). Ensemble and trajectory thermodynamics: A brief introduction. Physica A: Statistical Mechanics and its Applications 418, 6–16. 10.1016/j.physa.2014.04.035.

(S7) Astumian, R. D. (2018). Trajectory and Cycle-Based Thermodynamics and Kinetics of Molecular Machines: The Importance of Microscopic Reversibility. Acc. Chem. Res. 51, 2653–2661. 10.1021/acs.accounts.8b00253.

(S8) Hill, T. L. (1989). Free energy transduction and biochemical cycle kinetics (Springer-Verlag, New York).

(S9) Nam, K.-M.; Martinez-Corral, R.; Gunawardena, J. (2022). The linear framework: using graph theory to reveal the algebra and thermodynamics of biomolecular systems. Interface Focus 12, 20220013. 10.1098/rsfs.2022.0013.

(S10) King, E. L.; Altman, C. (1956). A Schematic Method of Deriving the Rate Laws for Enzyme-Catalyzed Reactions. J. Phys. Chem. A 60, 1375–1378. 10.1021/j150544a010.

(S11) Hill, T. L. (1966). Studies in irreversible thermodynamics IV. diagrammatic representation of steady state fluxes for unimolecular systems. J. Theor. Biol. 10, 442–459. 10.1016/0022-5193(66)90137-8.